 CMES, vol.5, no.3, pp.235-255, 2004

Multiscale Simulation Based on The Meshless Local Petrov-Galerkin (MLPG) Method

Shengping Shen[1] **and S. N. Atluri**[1]

Abstract: A multiscale simulation technique based on the MLPG methods, and finite deformation mechanics, is developed, implemented, and tested. Several alternate time-dependent interfacial conditions, between the atomistic and continuum regions, are systematically studied, for the seamless multiscale simulation, by decomposing the displacement of atoms in the equivalent-continuum region into long and short wave-length components. All of these methods for enforcing the interface conditions can ensure the passage of information accurately between the atomistic and continuum regions, while they lead to different performances at short wavelengths. The presently proposed Solution Method 2 reduces the phonon reflections at the interface, without increasing the computational burden. Multiple length scale, multiple time step, and meshless local Petrov-Galerkin (MLPG) methods are used in the numerical examples.

1 Introduction

With the advances in materials synthesis and device processing capabilities, the importance of developing and understanding nanoscale engineering devices has dramatically increased over the past decade. *Computational Nanotechnology* [Srivastava and Atluri (2002a,b)] has become an indispensable tool not only in predicting, but also in *engineering* the properties of multi-functional nano-structured materials. The elasto-dynamics is governed largely by the geometry of the device, while the atomistic processes are important in its smallest features. Continuum approaches begin to fail as the system size approaches the atomic scale, and atomistic methods begin to reach their inherent time and length-scale limitations. The nano-scale is the length scale of individual atoms, i.e. 1-10nm. At such length scales, continuum models are not flexible enough to accommodate the individual atomic scale processes. An alternative to continuum analysis is the atomistic modeling and simulation (MD), in which individual atoms are explicitly followed during their dynamic evolution. Even though this MD can trace all details of atomic-scale processes, it has its own set of limitations. When the length-scale cannot be accessed by either continuum methods because it is too small for averaging, or the atomistic methods [MD or quantum mechanics (QM)] because it is too large for simulations on the present day computers, these two approaches become inadequate, and that has presented significant challenges to the scientific community. The length scales of the typical material system in multi-scale structures are shown in Fig. 1.

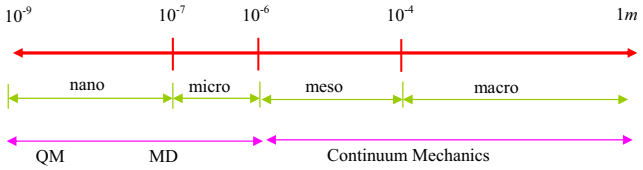

Figure 1 : The length scales of the material system

This paper is devoted to computational nanotechnology and multiscale simulations, in both length and time scales, as illustrated in Fig. 2, below [which is more fully discussed in Shen and Atluri (2004) and Atluri (2004)]. **Molecular Dynamics (MD) Domains, Equivalent Continuum Models (ECM), and Actual Continuum Domains (ACD)**, will be linked through the device of the Meshless Local Petrov-Galerkin (MLPG) Method [Atluri and Zhu(1998), and Atluri and Shen (2002a,b)], which is a cost-effective alternative to the traditional finite-element & boundary-element methods, and which offers the possibility of carrying out uniformly valid simulations of material properties for multi-scale systems at

[1] Center for Aerospace Research & Education
University of California at Irvine
5251 California Avenue, #140
Irvine, CA 92612, USA

both larger length scales and longer times than the direct atomistic calculations, and permits a reduction of the full set of atomic degrees of freedom.

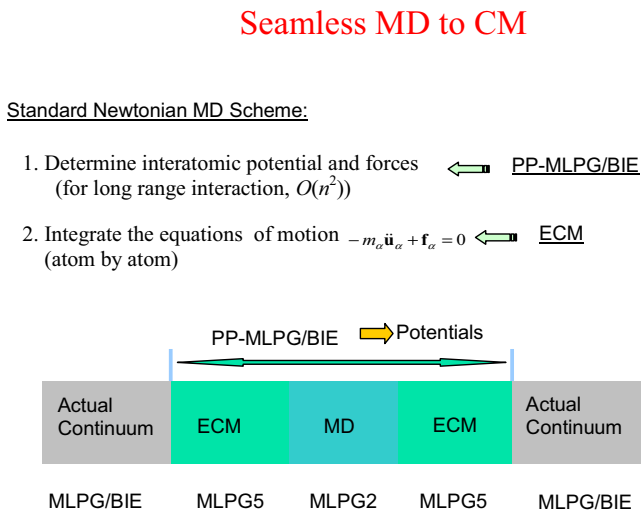

Figure 2 : Seamless Multiscale Modeling

The role of **computational nanotechnology** [Srivastava and Atluri (2002a,b); Srivastava, Menon, and Cho (2001)], has become critically important in the nanodevice development [Ajayan and Zhu(2001)]. There are two major categories of molecular simulation methods for nanotechnology: classical molecular dynamics (MD) and *ab initio* methods. MD treats the motion of atoms or molecules in approximated finite difference equations of Newtonian mechanics. In general, *ab initio* methods give more accurate results than MD, but they are also much more computationally intensive. A hybrid method, tight-binding molecular dynamics (TBMD), is a blend of certain features from both MD and *ab initio* methods. In fact, *ab initio* and TBMD are the quantum mechanics (QM) schemes. Despite constant increases in available computational power and improvement in numerical algorithms, even classical MD computations are still limited to simulating on the order of 10^6-10^8 atoms for a few nanoseconds. The simulation of large systems must be left to continuum methods. Several methods are developed for the multiscale simulation.

The quasicontinuum method, introduced by Tadmor et al. (1996), and Chung, Namburu, and Henz (2004), gives a theory for bridging the atomistic and continuum scales in *quasistatic problems*. In this method, a set of atoms making up a Bravais lattice is selected from a subset. *A triangulation of this subset allows the introduction of finite element-like shape functions at lattice points, allowing the interpolation of quantities at intermediate points in the lattice*. Thus, the problem of the minimization of energy to find equilibrium configurations can be written in terms of a reduced set of variables. The method is made practical by approximating summations over all atoms, as using summation rules analogous to numerical quadrature. The rules rely on the smoothness of the quantities over the size of the triangulation to ensure accuracy. The final aspect of the method is therefore the prescription of adaptivity rules, allowing the reselection of representative lattice points in order to tailor the computational mesh to the structure of the deformation field. The criteria for adaptivity are designed to allow full atomic resolution in regions of large local strain, for example, very close to a dislocation in the lattice. This method is limited to the case of a zero temperature.

Another approach to the coupling of the length scales is the FE/MD/TB model of Abraham (2000). In this method, three simulations are run simultaneously, using the finite element method (FEM), molecular dynamics (MD), and semi-empirical tight binding (TB). Each simulation is performed on a different region of the domain, with a coupling imposed in "handshake" regions where the different simulations overlap. The method is designed for implementation on supercomputers via parallel algorithms, allowing the solution of large problems. One example of such a problem is the propagation of a crack in a brittle material. Here, the TB method is used to simulate bond breaking at the crack tip, MD is used near the crack surface, and the surrounding medium is treated with FE. The challenge for mesh generation is that the mesh should smoothly transition between the true atomic lattice in the MD region and the closely-packed FE meshes. Too abrupt a crossover leads to an unphysical behavior, such as elastic wave resonances at the interface. The coarse-grained MD method proposed by Rudd and Broughton (1998) derived a constitutive relationship for the continuum, directly from the interatomic potential by using a statistical coarse graining procedure. This method has high computational complexity. Wagner and Liu (2003) presented a multiscale method for coupling molecular dynamics and continuum mechanics by using "bridging scale" decomposition and the quasicontinuum method [Tadmor et al. (1996)].

Although substantial progress has been made in recent

years, the multi-scale modeling method is still in its infancy, and it still requires intensive efforts. As pointed by many researchers, the main issues in the development of seamless multi-scale modeling methodology are still the limitations on the length and time scale, and the numerical accuracy and efficiency. Hence, a more accurate and efficient multi-scale modeling methodology is still desirable, and such methodologies are currently being pursued by many researchers, in contemporary literature. In this paper, we propose a seamless multi-scale modeling methodology, based on the meshless local Petrov-Galerkin (MLPG) method.

2 The Meshless Local Petrov-Galerkin (MLPG) Method and Radial Basis functions

Meshless methods, as alternative numerical approaches to eliminate the well-known drawbacks in the finite element and boundary element methods, have attracted much attention in recent decades, due to their flexibility, and due to their potential in negating the need for the human-labor intensive process of constructing geometric meshes in a domain

The MLPG method is a simple and less-costly alternative to the FEM and BEM [Atluri and Zhu (1998), Atluri and Shen (2002a,b)]. The main objective of the meshless methods is to get rid of, or at least alleviate the difficulty of, meshing and remeshing the entire structure; by only adding or deleting nodes in the entire structure, instead. The meshless local Petrov-Galerkin (MLPG) method is truly meshless, as no finite element/or boundary element meshes are required in this approach, either for purposes of interpolation of the trial and test functions for the solution variables, or for the purpose of integration of the 'energy'. All pertinent integrals can be easily evaluated over over-lapping, regularly shaped, domains (in general, spheres in three-dimensional problems) and their boundaries. Remarkable successes of the MLPG method have been reported in solving the convection-diffusion problems; fracture mechanics; Navier-Stokes flows; and plate bending problems. Recently, the MLPG method has made some strides, and it is applied successfully in studying strain gradient materials [Tang, Shen and Atluri, (2003)), three dimensional elasticity problems [Li, Shen, Han and Atluri (2003)], and elstodynamics [Batra, Ching (2002)]. The MLPG method was also extended to solve the boundary integral equations [Atluri, Han and Shen (2003), and Han, Atluri (2003)].

Six different nodal-based local test functions may be selected, which lead to six different MLPG methods. Based on the MLPG concept, these variants of the MLPG method are labeled as MLPG1, MLPG2, MLPG3, MLPG4, MLPG5, and MLPG6, respectively. Among them, there are three methods that avoid the domain integral in the weak-form, over the nodal test-function domain Ω_s: MLPG2 (wherein the local, nodal-based test function, over a local sub-domain Ω_s centered at a node, is a Dirac's Delta function); MLPG4 (wherein the local, nodal-based test function, over a local sub-domain Ω_s centered at a node, is the modified fundamental solution to the differential equation); and MLPG5 (wherein the local, nodal-based test function, over a local sub-domain Ω_s centered at a node, is the Heaviside step function). MLPG4 (which is synonymous with the Local Boundary Integral Equation method) involves singular integrals; while the collocation method, (i.e. MLPG2), is notorious for the sensitivity of the solution to the choice of proper collocation points. However, MLPG5 does not involve either a domain, or a singular integral, to generate the stiffness matrix; it only involves the regular boundary integral. Thus, it is a highly promising MLPG method while, numerical examples validate that the MLPG5 method is fast, accurate and robust.

In summary, the MLPG is a truly meshless method, which involves not only a meshless interpolation for the trial functions [such as MLS, PU, Shepard function or Radial Basis Functions(RBF)], but also a meshless integration of the weak-form (i.e. all integrations are always performed over regularly shaped sub-domains such as spheres, parallelepipeds, and ellipsoids in 3-D). In the conventional Galerkin method, the trial and test functions are chosen from the same function-space. In MLPG, the nodal trial and test functions can be different: the nodal trial function may correspond to any one of MLS, PU, Shepard function, or RBF types of interpolations; and the test function may be totally different, and may correspond to any one of MLS, PU, Shepard function, RBF, a Heaviside step function, a Dirac delta function, the Gaussian weight function of MLS, a special form of the fundamental solution to the differential equation, or any other convenient function, in the support domain, Ω_{te}, of the test function. Furthermore, the physical sizes of the supports (Ω_{tr} and Ω_{te}, respectively) of the nodal trial and test functions may be different. These features make the MLPG method very flexible. The MLPG method, based

on a local formulation, can include all the other meshless methods based on global formulation, as special cases [see Atluri, and Shen (2003)].

In this paper, we choose the local radial basis functions [Hardy (1971), Wendland (1999), Liu and Gu (2001)] to interpolate the trial functions, because of its Kronecker Delta property. Consider a continuous function $u(\mathbf{x})$ defined in a domain Ω, discretized by a set of nodes. An interpolation of $u(\mathbf{x})$ from the neighboring nodes of a point $\mathbf{x}_\alpha$ within the domain Ω, using RBFs augmented by a polynomial basis, can be written as

$$\begin{aligned} u(\mathbf{x}) &= \sum_{i=1}^{n} R_i(\mathbf{x})\, a_i(\mathbf{x}_\alpha) + \sum_{j=1}^{m} p_j(\mathbf{x})\, b_j(\mathbf{x}_\alpha) \\ &= \mathbf{R}^T\mathbf{a} + \mathbf{P}^T\mathbf{b} \end{aligned} \tag{1}$$

where $R_i(\mathbf{x})$ is the radial basis function, $p_j(\mathbf{x})$ is a monomial in the space coordinates, n is the number of nodes in the neighborhood of $\mathbf{x}_\alpha$, m is the number of polynomial basis functions (usually $m < n$), and $a_i(\mathbf{x}_\alpha)$ and $b_j(\mathbf{x}_\alpha)$ are the coefficients for $R_i(\mathbf{x})$ and $p_j(\mathbf{x})$, respectively, corresponding to the point $\mathbf{x}_\alpha$. The number of the neighbor nodes of $\mathbf{x}_\alpha$ is not greater than the total number of nodes in the global domain. The vectors are defined as

$$\begin{aligned} \mathbf{a}^T &= [a_1, a_2, \cdots, a_n] \\ \mathbf{b}^T &= [b_1, b_2, \cdots, b_m] \\ \mathbf{R}^T &= [R_1(\mathbf{x}), R_2(\mathbf{x}), \cdots, R_n(\mathbf{x})] \\ \mathbf{P}^T &= [p_1(\mathbf{x}), p_2(\mathbf{x}), \cdots, p_m(\mathbf{x})] \end{aligned} \tag{2}$$

The radial basis function has the following general form

$$R_i(\mathbf{x}) = R_i(r_i) \tag{3}$$

where $r_i = \|\mathbf{x} - \mathbf{x}_i\|$. The polynomial term is added to ensure the consistency and the condition of the non-singularity of the RBFs approximation, which should satisfy the following constraints

$$\sum_{i=1}^{n} p_j(\mathbf{x}_i)\, a_i = 0, \qquad j = 1, 2, \cdots, m \tag{4}$$

The coefficients are determined by ensuring that the interpolation passes through all n scattered nodes within the influence domain:

$$u(\mathbf{x}_k) = \sum_{i=1}^{n} R_i(\mathbf{x}_k)\, a_i + \sum_{j=1}^{m} p_j(\mathbf{x}_k)\, b_j, \qquad k = 1, 2, \cdots, n \tag{5}$$

Equations (5) and (4) can be expressed in matrix form

$$\mathbf{A}\left\{ \begin{array}{c} \mathbf{a} \\ \mathbf{b} \end{array} \right\} = \left\{ \begin{array}{c} \mathbf{u}_e \\ \mathbf{0} \end{array} \right\} \tag{6}$$

where

$$\mathbf{A} = \left[\begin{array}{cc} \mathbf{R}_0 & \mathbf{P}_0 \\ \mathbf{P}_0^T & \mathbf{0} \end{array} \right] \tag{7}$$

$$\mathbf{R}_0 = \left[\begin{array}{cccc} R_1(\mathbf{x}_1) & R_2(\mathbf{x}_1) & \cdots & R_n(\mathbf{x}_1) \\ R_1(\mathbf{x}_2) & R_2(\mathbf{x}_2) & \cdots & R_n(\mathbf{x}_2) \\ \vdots & \vdots & \vdots & \vdots \\ R_1(\mathbf{x}_n) & R_2(\mathbf{x}_n) & \cdots & R_n(\mathbf{x}_n) \end{array} \right]_{n\times n} \tag{8}$$

$$\mathbf{P}_0 = \left[\begin{array}{cccc} p_1(\mathbf{x}_1) & p_2(\mathbf{x}_1) & \cdots & p_m(\mathbf{x}_1) \\ p_1(\mathbf{x}_2) & p_2(\mathbf{x}_2) & \cdots & p_m(\mathbf{x}_2) \\ \vdots & \vdots & \vdots & \vdots \\ p_1(\mathbf{x}_n) & p_2(\mathbf{x}_n) & \cdots & p_m(\mathbf{x}_n) \end{array} \right]_{n\times m} \tag{9}$$

$$\mathbf{u}_e = [u_1, u_2, \cdots, u_n]^T \tag{10}$$

Then, from equation (6), the coefficients can be obtained. Finally, the interpolation is expressed as

$$u(\mathbf{x}) = \left[\begin{array}{cc} \mathbf{R}^T(\mathbf{x}) & \mathbf{P}^T(\mathbf{x}) \end{array} \right] \mathbf{A}^{-1} \left\{ \begin{array}{c} \mathbf{u}_e \\ \mathbf{0} \end{array} \right\} = \boldsymbol{\phi}(\mathbf{x})\, \mathbf{u}_e \tag{11}$$

where the matrix of the shape functions $\phi(\mathbf{x})$ is defined by

$$\boldsymbol{\phi}(\mathbf{x}) = \left[\phi^1(\mathbf{x}), \phi^2(\mathbf{x}), \cdots, \phi^i(\mathbf{x}), \cdots, \phi^n(\mathbf{x}) \right] \tag{12}$$

with

$$\phi^k(\mathbf{x}) = \sum_{i=1}^{n} R_i(\mathbf{x})\, \hat{\mathbf{A}}_{ik} + \sum_{j=1}^{m} p_j(\mathbf{x})\, \hat{\mathbf{A}}_{(n+j)k} \tag{13}$$

where $\hat{\mathbf{A}}_{ik}$ represents the (i,k) element of matrix $\mathbf{A}^{-1}$.

The widely used RBFs include multiquadrics (MQ), Gaussian (EXP), and thin plate splines (TPS) forms, and so on. In this paper, we will employ the multiquadrics (MQ) form:

$$R_i(\mathbf{x}) = \left(r_i^2 + c^2\right)^{\beta} \tag{14}$$

c and β are the shape parameters. Here, we choose $c = 1$, $\beta = 1.03$ or $c = 2$, $\beta = 1.99$.

3 The MLPG Method for Multiscale Simulation

In this section, a finite deformation model based on the atomistic physics will be developed, for use in the ECM region.

In continuum mechanics, the stress at a material point is a function of the 'state' variables, such as strain, and its gradients, at the same point. In order to formulate a constitutive law for an *equivalent continuum model* (ECM) from the atomic forces, a hypothesis to connect the continuum displacement field and the motions of atoms must be employed. The Cauchy-Born hypothesis is the basis for developing the ECM elastic potentials, from the atomistic description of the system. In the absence of slips, phase transitions, twinning or other inelastic phenomena, the Cauchy-Born hypotheses for crystals are equivalent for homogeneous deformations (Ericksen, 1984). Once the geometry of the deformed lattice vectors is linked to the continuum deformation, a constitutive model based on atomistic description can be constructed by equating the continuum strain energy density to the potential energy of the atomic system for a representative cell, divided by its volume, as in Tadmor et al. (1996).

In this paper, first, we will develop an MLPG tangent-stiffness method for the ECM region, in which it is assumed that the state of deformation is homogeneous and can be well-characterized by the local deformation gradient **F**. The inhomogeneous deformation, such as near defect cores, will be accounted for by the pure molecular dynamics (MD). The whole idea is that: in the ECM, MLPG5 or MLPG1 tangent-stiffness method will be employed; in the MD region, MLPG2 tangent-stiffness method will be employed.

Both of these, the ECM and MD regions, will be linked through the device of the meshless local Petrov-Galerkin (MLPG) method, which will thus offer the possibility of carrying out uniformly valid simulations of material properties for multi-scale systems at both larger length scales and longer times than direct atomistic calculations, and permits a reduction of the full set of atomic degrees of freedom; thus inching towards almost $O(N)$ algorithms. This is illustrated of in Fig. 3. In the ECM region, the nodes can be taken to be arbitrary, and not necessarily be coincident with the atoms. In MD region, the nodes are taken to be the atoms themselves. In the ECM region, the solid points represent the atoms, while the open points represent the nodes of the MLPG method. MLPG5 will be implemented in "ECM" region and MLPG2 will be implemented in MD region.

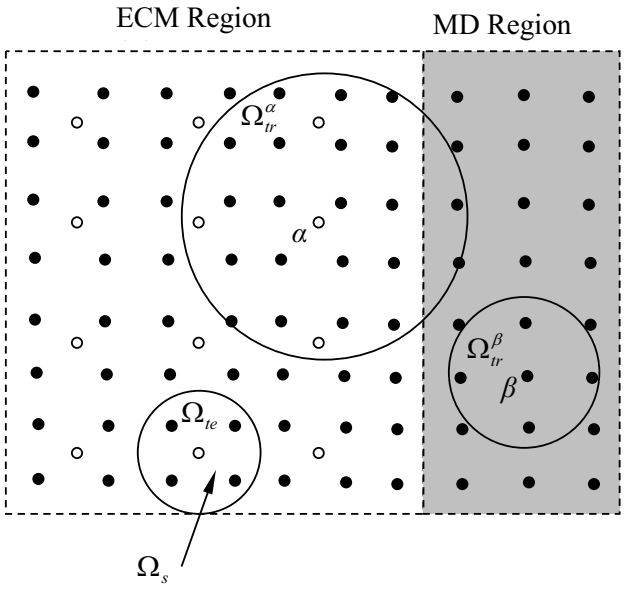

Figure 3 : Illustration of multiscale simulation.

The dynamic motion for atomic positions are governed by Newtonian mechanics and described by molecular dynamics. The multi-scale materials are discritized into a set of nodes. In the molecular dynamics region, the position of the atom can be interpolated by the meshless interpolation (the moving least square or radial basis functions) of the nodes, similar to the displacement in the continuum mechanics region. The atomic forces are analytic derivatives of the inter-atomic potential (Born-Oppenheimer expansion). In the ECM, the atomic environment is characterized by the deformation gradient there. *Each continuum point is taken to represent a large region on the atomic scale, which is homogeneously distorted according to the deformation gradient at the point.* The constitutive response in this region is obtained from the atomistic calculation rather than a phenomenological rule, in a way similar to the quasicontinuum method proposed by Tadmor et al. (1996), and Chung, Namburu, and Henz (2004).

By means of the concept of the MLPG, a local weak form (in subdomain Ω_s, as in Fig. 3) for the Newton's law of motion (conservation of linear momentum) will be used to derive a system of equations for multi-scale materials

modeling. In this paper, we choose radial basis function to be the interpolation scheme, due to its convenience in this case and their Kroneck Delta property [Atluri & Shen, (2002a, b, 2003)].

In classical continuum mechanics, a point $\mathbf{X}$ in the undeformed body Ω_0 in the reference frame is mapped to a point $\mathbf{x}$ in its current shape Ω in the current frame. The deformed configuration of the body is described by a displacement function $\mathbf{u}(\mathbf{X})$, which represents the displacement at point $\mathbf{X}$, as

$$\mathbf{x} = \mathbf{X} + \mathbf{u}(\mathbf{X})$$

The deformation gradient is defined by

$$\mathbf{F} = \frac{\partial \mathbf{x}}{\partial \mathbf{X}} = \mathbf{I} + \frac{\partial \mathbf{u}}{\partial \mathbf{X}}$$

to map infinitesimal material vector from the undeformed body Ω_0 into the deformed one Ω. Here, $\mathbf{I}$ is the identity tensor.

In the molecular dynamics region, the initial position of an atom I is denoted as $\mathbf{X}_I$. The current configuration of the atom is described by a displacement $\mathbf{u}$ which depends on $\mathbf{X}$, and can be written as

$$\mathbf{x}_I = \mathbf{X}_I + \mathbf{u}_I \tag{15}$$

where $\mathbf{u}_I$=$\mathbf{u}(\mathbf{X}_I)$.

The distance between two atoms I and J in the reference configuration can be written as

$$\mathbf{R}_{IJ} = \mathbf{X}_J - \mathbf{X}_I \tag{16}$$

The distance between two atoms I and J in the current configuration can be written as

$$\mathbf{r}_{IJ} = \mathbf{x}_J - \mathbf{x}_I \tag{17}$$

According to the Cauchy-Born rule (Ericksen, 1984), for simple Bravais lattice that has the centrosymmetric atomic structure, we have

$$\mathbf{r}_{IJ} = \mathbf{F}\mathbf{R}_{IJ} \tag{18}$$

However, it does not hold for a complex Bravais lattice, which can be described by be means of a number of interpenetrating simple Bravais lattices (sub-lattices) and does not possess centrosymmetry, such as the hexagonal lattice. In this case, the Cauchy-Born rule gives [Zanzotto (1996), Martin (1975), Cousins (1978), Born and Huang (1954)]

$$\mathbf{r}_{IJ} = \mathbf{F}\mathbf{R}_{IJ} + \boldsymbol{\varsigma}_k \tag{19}$$

where the internal variables $\boldsymbol{\varsigma}_k$ are shift vectors, with k ranging from 0 to some integer N (There are N+1 sublattices in the complex Bravais lattice. If atoms I, J are in the same sub-lattices, $\boldsymbol{\varsigma}_k = 0$). $\boldsymbol{\varsigma}_k$ and $\mathbf{F}$ are independent variables. At the static equilibrium state, the vectors $\boldsymbol{\varsigma}_k$ are to be determined by the minimization of the energy function, so as to reach an equilibrium configuration in the deformed crystal. This means that the equilibrium values of $\boldsymbol{\varsigma}_k$ can be written as functions of $\mathbf{F}$. In this paper, which focuses on dynamical problems, we will avoid making any specific hypothesis on the behavior of $\boldsymbol{\varsigma}_k$. As discussed later [see equation (98)], what we need is $\partial \mathbf{r}_{IJ} / \partial \mathbf{F} = \mathbf{R}_{IJ}$ from either (18) or (19).

It is noted that, in order to apply the Cauchy-Born rule to nanotubes or fullerenes, a more general exponential mapping procedure like the one in Arroyo and Belytchko (2002) should be used. That will be taken into account as we apply the present multiscale simulation to nanotubes.

The right Cauchy-Green strain tensor is defined by

$$\mathbf{C} = \mathbf{F}^T \mathbf{F} \tag{20}$$

and the Green strain tensor is defined by

$$\mathbf{E} = \frac{1}{2}(\mathbf{C} - \mathbf{I}) \tag{21}$$

The kinematics of the deformation is characterized by the deformation gradient. The constitutive nature of the material is obtained through the strain energy density function W which relates the energy at a point to the local state of deformation there. It may be shown that W can only be a function of $\mathbf{F}$, from the hypothesis of locality and use the entropy production inequality. Moreover, according to the postulate of material frame indifference, it can be shown that the dependence of W on $\mathbf{F}$ can only be through the right Cauchy-Green tensor $\mathbf{C}$.

Following the classical continuum mechanics, the second Piola-Kirchhoff stress $\mathbf{S}$ can be defined as

$$\mathbf{S} = \frac{\partial W}{\partial \mathbf{E}} = 2\frac{\partial W}{\partial \mathbf{C}} \tag{22}$$

C and **S** are invariant with respect to rigid-body rotation.

The conservation of linear momentum leads to:

$$\nabla \cdot \left(\mathbf{S}\mathbf{F}^T\right) + \mathbf{f} = \rho \mathbf{w} \tag{23}$$

where $\nabla\cdot$ denotes the divergence taken with respect to the material frame, $\mathbf{f}$ is the body force, ρ is the density, and $\mathbf{w}$ is the acceleration, i.e., $\mathbf{w} = \frac{d^2\mathbf{u}}{dt^2}$.

The conservation of angular momentum leads to:

$$\mathbf{S} = \mathbf{S}^T \tag{24}$$

The tangent stiffness material-moduli can be defined as

$$\mathbf{D} = \frac{\partial^2 W}{\partial \mathbf{E} \partial \mathbf{E}} = 4\frac{\partial^2 W}{\partial \mathbf{C} \partial \mathbf{C}} \tag{25}$$

More details about the finite strain analysis can be found in Atluri (1979, 1980).

The *local weak form* of equation (23) can be written as

$$\int_{\Omega_s} \left[\nabla \cdot \left(\mathbf{S}\mathbf{F}^T\right) + \mathbf{f} - \rho \mathbf{w}\right] \mathbf{V} d\Omega = 0 \tag{26}$$

where $\mathbf{V}$ is the test function in the local domain Ω_s. The local symmetric weak form can be written as

$$\begin{aligned} &\int_{\Omega_s} (S_{KL} x_{l,L}) V_{l,K} d\Omega + \int_{L_s} S_{KL} x_{l,L} n_K V_l d\Gamma \\ &\quad + \int_{\Gamma_{su}} S_{KL} x_{l,L} n_K V_l d\Gamma \\ &= \int_{\Gamma_{st}} S_{KL} x_{l,L} n_K V_l d\Gamma + \int_{\Omega_s} (f_l - \rho w_l) V_l d\Omega \end{aligned} \tag{27}$$

where $\mathbf{n}$ is the unit normal to the local boundary surface Γ_s of Ω_s. The corresponding MLPG5 weak-form (when the test functions are taken to Heaviside functions) is :

$$\begin{aligned} &\int_{L_s} S_{KL} x_{l,L} n_K d\Gamma + \int_{\Gamma_{su}} S_{KL} x_{l,L} n_K d\Gamma \\ &= \int_{\Gamma_{st}} S_{KL} x_{l,L} n_K d\Gamma + \int_{\Omega_s} (f_l - \rho w_l) d\Omega \end{aligned} \tag{28}$$

Actually, the *MLPG5 [equation (28)] can be directly derived from the conservation of linear momentum in an arbitrary local domain, which is the basis of the finite deformation theory.* The physical basis of the MLPG5 is the conservation of linear momentum in an arbitrary local domain, and that of the MLPG2 is the conservation of linear momentum on arbitrary point.

A corresponding continuous interpolation will replace the piece-wise function for the position of the atom in the ECM region,

$$\mathbf{x} = \sum_{\alpha=1}^{N} \phi^{\alpha}(\mathbf{X}) \mathbf{x}_{\alpha} \tag{29}$$

$\mathbf{x}_{\alpha}, \alpha = 1, 2, \ldots, N$, in equation (29), are the nodal values. $\phi^{\alpha}(\mathbf{X})$ is the RBF shape function.

Assume that there are N_1 atoms in region A (MD), and N_2 in region B (ECM). The displacements of atoms I in the Region A are denoted by $\mathbf{q}_I$ $(1 \le I \le N_1)$. The displacements of *atom i* in the Region B are denoted by $\mathbf{u}_i$ $(1 \le i \le N_2)$, which are interpolated from the displacements of the *nodes* in region B, as

$$\mathbf{u}_i = \mathbf{u}(\mathbf{X}_i) = \sum_{\alpha=1}^{N} \phi^{\alpha}(\mathbf{X}_i) \mathbf{u}_{\alpha} \tag{30}$$

Here, $\mathbf{u}_{\alpha}$, α=1, 2,..., N, are the nodal values. It is noted that N is less than the amount of atoms of Region B, i.e., $N \le N_2$, and the node is not necessarily an atom. The displacement $\mathbf{u}_i$ of an atom in region B implies an average value of the atomic displacement, and can not catch the thermal fluctuations.

3.1 The Atomistic Constitutive Law for Homogeneous Deformation and MLPG5, in ECM

The classical MD describes the system's atomic-scale dynamics, where atoms and molecules move, while interacting with many of the atoms and molecules in the vicinity. The system's dynamic evolution is governed by Hamilton's classical equation of motion from Newton's second law. Each atom moves and acts simply as a particle that is moving in a many-body force field of other similar particles. The atomic and molecular interactions describing the dynamics are thus given by classical many-body force-field functions, and the interatomic potential Π as an infinite sum over pair, triplet, etc., can be expressed by the Born-Opennheimer expansion as:

$$\begin{aligned} \Pi = \sum_I \Bigg[&\frac{1}{2!} \sum_{J \neq l} V^{(2)}(\mathbf{r}_{IJ}) + \frac{1}{3!} \sum_{K \neq} \sum_{J \neq I} V^{(3)}(\mathbf{r}_{IJ}, \mathbf{r}_{KI}, \mathbf{r}_{KJ}) \\ &+ \cdots + \frac{1}{n!} \sum_{L \neq} .. \sum_{M \neq} .. \sum_{J \neq l} V^{(n)}(\mathbf{r}_{IJ}, \cdots, \mathbf{r}_{IL}, \cdots, \mathbf{r}_{ML}, \cdots) \Bigg] \end{aligned} \tag{31}$$

$V^{(2)}$, $V^{(3)}$ ... and $V^{(n)}$ are the interaction potentials of the two-, three- and *n*-body interactions, respectively.

As an example, we consider a two-body and three-body separable potential here. The energy can be expressed as,

$$\Pi = \sum_I \left[\frac{1}{2} \sum_{J \neq l} V^{(2)}(\mathbf{r}_{IJ}) + \sum_{K \neq} \sum_{J \neq I} V^{(3)}(\mathbf{r}_{IJ}, \mathbf{r}_{Ik}, \mathbf{r}_{Jk}) \right] \quad (32)$$

In this paper, an important procedure is to estimate the strain energy density in the ECM If we sum over all the atoms as in the classical molecular dynamics, we can certainly get the energy density by evaluating Π / Ω. However, this is very expensive. In the quasicontinuum method [Tadmor et al. (1996)], for a homogeneously distorted crystal, the continuum strain energy density is obtained by equaling to the potential energy of the atomic system for a representative cell divided by its volume, which means that the calculation of equation (32) is limited *to a single unit cell*. This method will be used in regions that are very far from the inhomogeneous region, in this paper. *In the MLPG method, it is natural to limit the calculation of equation (32) to a local domain* Ω_s, ie.,

$$W = \frac{1}{\Omega_s} \sum_{I \in \Omega_s} \left[\frac{1}{2} \sum_{J \neq l} V^{(2)}(\mathbf{r}_{IJ}) + \sum_{K \neq} \sum_{J \neq I} V^{(3)}(\mathbf{r}_{IJ}, \mathbf{r}_{Ik}, \mathbf{r}_{Jk}) \right] - \frac{\Pi_r}{\Omega_s} = \frac{\Pi_s}{\Omega_s} \quad (33)$$

where Ω_s is the volume of the local domain, and Π_r is the potential energy of the reference configuration. It is noted that the atoms *K* and *J* are located in the local domain Ω_s, and within the cutoff radius of the boundary of the local domain Ω_s. It is noted that both the interatomic potential energy and the strain energy, involve reference states. The former is referenced to infinitely separated atoms, and the latter is referenced to the unstrained configuration. Hence, the constant offset energy Π_r, representing the potential energy in the unstrained state, which does not affect the dynamics is subtracted in equation (33).

If the energy can be written in a form that is additively decomposed, such that $\Pi = \sum_{I=1} \Pi_I$, with Π_I denotes the potential energy for each atom, another way to derive the strain energy density is to assume that each atom can be assigned a volume $\Delta\Omega_I$ in the undeformed configuration ($\Omega = \sum_{I=1} \Delta\Omega_I$). Then, the strain energy density can be derived as $W = \Pi_I / \Delta\Omega_I$. In our numerical examples, we proceed in this way.

After obtaining the strain energy density (33) by the Cauchy-Born rule, the second Piola-Kirchhoff stress **S,** and the tangent stiffness moduli **D,** in the ECM can be expressed, respectively, as

$$\begin{aligned} \mathbf{S} &= \frac{\partial W}{\partial \mathbf{E}} = \frac{2}{\Omega_s} \frac{\partial \Pi_s}{\partial \mathbf{C}} \\ &= \frac{2}{\Omega_s} \sum_{I \in \Omega_s} \left[\frac{1}{2} \sum_{J \neq l} \frac{\partial V^{(2)}(\mathbf{r}_{IJ})}{\partial \mathbf{r}_{IJ}} \frac{\partial \mathbf{r}_{IJ}}{\partial \mathbf{C}} \right] \\ &\quad + \frac{2}{\Omega_s} \sum_{I \in \Omega_s} \left[\sum_{K \neq} \sum_{J \neq I} \frac{\partial V^{(3)}(\mathbf{r}_{IJ}, \mathbf{r}_{Ik}, \mathbf{r}_{Jk})}{\partial \mathbf{r}_{IJ}} \frac{\partial \mathbf{r}_{IJ}}{\partial \mathbf{C}} \right. \\ &\quad + \frac{\partial V^{(3)}(\mathbf{r}_{IJ}, \mathbf{r}_{Ik}, \mathbf{r}_{Jk})}{\partial \mathbf{r}_{Ik}} \frac{\partial \mathbf{r}_{Ik}}{\partial \mathbf{C}} \\ &\quad \left. + \frac{\partial V^{(3)}(\mathbf{r}_{IJ}, \mathbf{r}_{Ik}, \mathbf{r}_{Jk})}{\partial \mathbf{r}_{Ik}} \frac{\partial \mathbf{r}_{Jk}}{\partial \mathbf{C}} \right] \end{aligned} \quad (34)$$

$$\mathbf{D} = 4 \frac{\partial^2 W}{\partial \mathbf{C} \partial \mathbf{C}} = \frac{4}{\Omega_s} \frac{\partial^2 \Pi_s}{\partial \mathbf{C} \partial \mathbf{C}} \quad (35)$$

where

$$\frac{\partial \mathbf{r}_{IJ}}{\partial \mathbf{F}} = \mathbf{R}_{IJ}, \quad \frac{\partial \mathbf{F}}{\partial \mathbf{C}} = \mathbf{F}^{-1}, \quad \frac{\partial \mathbf{r}_{IJ}}{\partial \mathbf{C}} = \mathbf{R}_{IJ} \mathbf{F}^{-1} \quad (36)$$

The equations from the nonlinear local Petrov-Galerkin formulation (27), can be solved by employing an incremental algorithm. The total Lagrangean method (T. L.) will be employed in this paper. Assuming that the equation (27) is at time *t*, then from time *t* to time $t + \Delta t$, the incremental constitutive relation in the ECM can be expressed as

$$\Delta \mathbf{S} = \mathbf{D} : \Delta \mathbf{E} = \mathbf{D} : \left(\nabla \Delta \mathbf{u} + \nabla \mathbf{u}^T \cdot \nabla \Delta \mathbf{u} \right) \quad (37a)$$

or

$$\Delta S_{KL} = D_{KLMN} \left(\Delta u_{M,N} + u_{P,M} \Delta u_{P,N} \right) \quad (37b)$$

where $\Delta \mathbf{u}$ is the discernment of the displacement, i.e.,

$$\Delta \mathbf{u} = {}^{t+\Delta t}\mathbf{u} - {}^{t}\mathbf{u} \quad (38)$$

with ${}^t\mathbf{u}$ denotes the displacement $\mathbf{u}$ at time t. The equation (27) at time $t+\Delta t$ can be linearized as

$$\int_{\Omega_s} \Delta\left(S_{KL}x_{l,L}\right) V_{l,K} d\Omega + \int_{L_s} \Delta\left(S_{KL}x_{l,L}\right) n_K V_l d\Gamma + \int_{\Gamma_{su}} \Delta\left(S_{KL}x_{l,L}\right) n_K V_l d\Gamma - \int_{\Omega_s} \rho\left({}^t w_l + \Delta w_l\right) V_l d\Omega = Q \tag{39}$$

where the density is defined as

$$\rho = \frac{1}{\Omega_s}\sum_{I\in\Omega_s}^{m_I} \quad \text{or} \quad \rho = \frac{m_I}{\Delta\Omega_I} \tag{40}$$

and

$$\begin{aligned} Q = &\int_{\Gamma_{st}} S_{KL}x_{l,L} n_K V_l d\Gamma + \int_{\Omega_s} f_l V_l d\Omega \\ &+ \int_{\Gamma_{st}} \Delta\left(S_{KL}x_{l,L}\right) n_K V_l d\Gamma + \int_{\Omega_s} \Delta f_l V_l d\Omega \\ &- \int_{\Omega_s} S_{KL}x_{l,L} V_{l,K} d\Omega - \int_{L_s} S_{KL}x_{l,L} n_K V_l d\Gamma \\ &- \int_{\Gamma_{su}} S_{KL}x_{l,L} n_K V_l d\Gamma \end{aligned} \tag{41}$$

If we adopt the MLPG5 method, equation (39) and (41) can be rewritten as

$$\int_{L_s} \Delta\left(S_{KL}x_{l,L}\right) n_K d\Gamma + \int_{\Gamma_{su}} \Delta\left(S_{KL}x_{l,L}\right) n_K d\Gamma - \int_{\Omega_s} \rho\left({}^t w_l + \Delta w_l\right) d\Omega = Q_l \tag{42}$$

and

$$\begin{aligned} Q_l = &\int_{\Gamma_{st}} S_{KL}x_{l,L} n_K d\Gamma + \int_{\Omega_s} f_l d\Omega + \int_{\Gamma_{st}} \Delta\left(S_{KL}x_{l,L}\right) n_K d\Gamma \\ &+ \int_{\Omega_s} \Delta f_l d\Omega - \int_{L_s} S_{KL}x_{l,L} n_K d\Gamma - \int_{\Gamma_{su}} S_{KL}x_{l,L} n_K d\Gamma \end{aligned} \tag{43}$$

By using the natural boundary on Γ_t, $S_{KL}x_{l,L}n_K = \overline{T}_l$, equation (43) can be written as

$$\begin{aligned} Q_l = &\int_{\Gamma_{st}} \overline{T}_l d\Gamma + \int_{\Omega_s} f_l d\Omega + \int_{\Gamma_{st}} \Delta\overline{T}_l d\Gamma + \int_{\Omega_s} \Delta f_l d\Omega \\ &- \int_{L_s} S_{KL}x_{l,L} n_K d\Gamma - \int_{\Gamma_{su}} S_{KL}x_{l,L} n_K d\Gamma \end{aligned} \tag{44}$$

According to equation (37), equation (39) or (42) is a linear equation in terms of $\Delta\mathbf{u}$. The increment of displacement, $\Delta\mathbf{u}$, can be interpolated in the MLPG method as

$$\Delta\mathbf{u} = \sum_{\alpha=1}^{N} \phi^{\alpha}(\mathbf{X})\,\Delta\mathbf{u}_{\alpha} \tag{45}$$

$\Delta\mathbf{u}_{\alpha}, \alpha = 1, 2, \ldots, N$, in equation (45), are the nodal values. Again, it is noted that N is less than the amount of atoms of the system, and the node is not necessarily the atom. For convenience, we rewrite equation (45) as

$$\Delta u_I = \sum_{\alpha=1}^{N} \phi_{IJ}^{\alpha}(\mathbf{X})\,\Delta u_{\alpha J} \tag{46}$$

with $\phi_{IJ}^{\alpha} = \phi^{\alpha}\delta_{IJ}$.

Substitution of equation (45) into equation (42), for all nodes, leads to the following discretized system of linear equations:

$$-\sum_{\beta=1}^{N}\left[\mathbf{M}_{\alpha\beta}{}^{t+\Delta t}\ddot{\mathbf{u}}_{\beta}\right] + \sum_{\beta=1}^{N}\left[{}^t\mathbf{K}_{\alpha\beta}\Delta\mathbf{u}_{\beta}\right] = \mathbf{Q}_{\alpha} \tag{47}$$

where

$$\begin{aligned} &\left[{}^t\mathbf{K}_{\alpha\beta}\right]_{JI} \\ &= \int_{L_s}\Big[D_{KLMN}\left(\delta_{JL} + {}^t u_{J,L}\right) n_K \left(\delta_{PM} + {}^t u_{P,M}\right)\phi_{PI,N}^{\beta} \\ &\quad + S_{KL}n_K\phi_{JI,L}^{\beta}\Big]\,d\Gamma \\ &\quad + \int_{\Gamma_{su}}\Big[D_{KLMN}\left(\delta_{JL} + {}^t u_{J,L}\right) n_K \left(\delta_{PM} + {}^t u_{P,M}\right)\phi_{PI,N}^{\beta} \\ &\quad + S_{KL}n_K\phi_{JI,L}^{\beta}\Big]\,d\Gamma \end{aligned} \tag{48}$$

$$\left[\mathbf{M}_{\alpha\beta}\right]_{JI} = \int_{\Omega_s}\rho\phi_{JI}^{\beta}d\Omega \tag{49}$$

$$\begin{aligned} &\{\mathbf{Q}_{\alpha}\}_J \\ &= \int_{\Gamma_{st}}\overline{T}_J d\Gamma + \int_{\Omega_s} f_J d\Omega + \int_{\Gamma_{st}}\Delta\overline{T}_J d\Gamma + \int_{\Omega_s}\Delta f_J d\Omega \\ &\quad - \int_{L_s} S_{KL}\left(\delta_{JL} + {}^t u_{J,L}\right) n_K d\Gamma \\ &\quad - \int_{\Gamma_{su}} S_{KL}\left(\delta_{JL} + {}^t u_{J,L}\right) n_K d\Gamma \end{aligned} \tag{50}$$

The integration in equation (48)-(50) can employ the Gaussian quadrature. It is shown that no domain integration in involved in equation (48), which is an important advantage of MLPG5.

The linearized equations (47) will be very effective for static or implicit time integration schemes. However, if an explicit time integration scheme is employed, we can directly use equations (28), and do not need to linearize them. In this paper, we will use the central difference rule to integrate time, and not linearize equations (28).

In this case, equation (28) can be rewritten as

$$\mathbf{M}_{\alpha\beta}\ddot{\mathbf{u}}_\beta = \mathbf{t}_\alpha \tag{51}$$

for node α or

$$\mathbf{M}_C\ddot{\mathbf{d}} = \mathbf{t}_C \tag{52}$$

for the whole region B, with

$$\begin{aligned}
&\mathbf{t}_\alpha \\
&= \int_{\Gamma_{st}} \left(\mathbf{S}\mathbf{F}^T\right)\cdot\mathbf{n}d\Gamma - \int_{L_s} \left(\mathbf{S}\mathbf{F}^T\right)\cdot\mathbf{n}d\Gamma - \int_{\Gamma_{su}} \left(\mathbf{S}\mathbf{F}^T\right)\cdot\mathbf{n}d\Gamma \\
&= \int_{\Gamma_{st}} \frac{\partial W}{\partial \mathbf{F}}\cdot\mathbf{n}d\Gamma - \int_{L_s} \frac{\partial W}{\partial \mathbf{F}}\cdot\mathbf{n}d\Gamma - \int_{\Gamma_{su}} \frac{\partial W}{\partial \mathbf{F}}\cdot\mathbf{n}d\Gamma
\end{aligned} \tag{53}$$

$$\mathbf{M}_{\alpha\beta} = \int_{\Omega_s} \rho\phi^\beta \mathbf{I}d\Omega \tag{54}$$

and

$$\mathbf{d} = [\mathbf{u}_1, \mathbf{u}_2, \cdots, \mathbf{u}_\alpha, \cdots, \mathbf{u}_N]^T$$
$$\mathbf{t}_C = [\mathbf{t}_1, \mathbf{t}_2, \cdots, \mathbf{t}_\alpha, \cdots, \mathbf{t}_N]^T$$

Gaussian quadrature is employed to compute the integral in equation (53) numerically. $\mathbf{M}_{\alpha\beta}$ is the sub-matrix of the global mass matrix $\mathbf{M}_C$ in region B. Here, the body force is not considered. Equation (54) is for the consistent mass matrix. It is noted that we can also use the lumped mass in equation (52) same as that in FEM. The lumping procedure can be same as that in FEM. Then, we will obtain a diagonal mass matrix. Actually, in MLPG method, to lump the mass matrix is simpler and more convenient than in FEM, we can just assign the mass on the node instead of distributing it continuously within the local domain, i.e.

$$\rho = \overline{m}_\alpha \delta(\mathbf{X} - \mathbf{X}_\alpha) \tag{55}$$

with $\overline{m}_\alpha = \int_{\Omega_s} \rho d\Omega$. Then, we have the diagonal mass matrix

$$\mathbf{M}_{\alpha\beta} = \overline{m}_\alpha \delta_{\alpha\beta}\mathbf{I} \tag{56}$$

This reduces to the correct description in the atomic limit, where nodes coincide with atoms. It is noted that equation (56) can also be obtained by means of the row-sum technique, because of the zero-order consistency, i.e., $\sum_{\beta=1}^{n} \phi^\beta = 1$.

4 Atomistic (MD) Simulation in the Inhomogeneous Deformation Region

In the inhomogeneous-deformation region, we will employ the MLPG2 by letting the node to be the atom itself. Assume that there are N_1 atoms in this region (MD). The displacement of atom I in this region is denoted as $\mathbf{q}_I$ $(1 \le I \le N_1)$. Now, the control equation will be

$$-m_I\ddot{\mathbf{q}}_I + \mathbf{f}_I = 0 \tag{57}$$

$$\mathbf{f}_I = -\frac{\partial \Pi}{\partial \mathbf{x}_I} = -\frac{\partial \Pi}{\partial \mathbf{q}_I} \tag{58}$$

The force $\mathbf{f}_I$ is computed, as it would be in a standard atomistic calculation. In molecular dynamics, these equations are approximated as finite-difference equations with discrete time step Δt and are solved by the standard Gear's fifth-order predictor-corrector or Verlet's leapfrog method. The evaluation of the interatomic potential energy, and forces, is performed by taking advantage of the neighbor-list of atoms, so that the time for the computation scales with the number of atoms in region A, i.e. it is of order-N_1. The neighbor list is renewed every several time steps.

Similar to that in section 3, we can also linearize equation (57). Although we will not employ it in the numerical examples, we still list the equations here. Equation (57) can be rewritten as

$$-m_I{}^{t+\Delta t}\ddot{\mathbf{q}}_I + {}^{t+\Delta t}\mathbf{f}_I = 0 \tag{59}$$

Then, equation (59) is written as

$$\begin{aligned}
&-m_I{}^{t+\Delta t}\ddot{\mathbf{q}}_I + {}^{t+\Delta t}\mathbf{f}_I \\
&\approx -m_I{}^{t+\Delta t}\ddot{\mathbf{q}}_I + {}^{t}\mathbf{f}_I + \sum_{J=1}{}^{t}\left(\frac{\partial \mathbf{f}_I}{\partial \mathbf{q}_J}\right)\Delta\mathbf{q}_J = 0
\end{aligned} \tag{60}$$

The above equation can be rewritten as

$$-m_I {}^{t+\Delta t}\ddot{\mathbf{q}}_I + \sum_{J=1}^{N} \left[{}^{t}\mathbf{K}_{IJ} \Delta \mathbf{q}_J \right] = \Delta \mathbf{Q}_I \tag{61}$$

where the tangent stiffness matrix ${}^{t}\mathbf{K}_{IJ}$ is defined as

$${}^{t}\mathbf{K}_{IJ} = \frac{\partial \mathbf{f}_I}{\partial \mathbf{q}_J} \tag{62}$$

and

$$\Delta \mathbf{Q}_I = -{}^{t}\mathbf{f}_I \tag{63}$$

Now, a unified formulation for the multiscale system can be developed, based on the MLPG method , and the tangent stiffness concept. The equation (47) and (61) can be written as

$$\mathbf{M}^{t+\Delta t}\ddot{\mathbf{u}} + {}^{t}\mathbf{K}\Delta \mathbf{u} = {}^{t+\Delta t}\mathbf{Q} \tag{64}$$

This method should be very effective due to the fact that adaptive remeshing, which is an important factor in multiscale dynamics, is very convenient in the MLPG method. This computational methodology provides a unified method for simulation in MD and equivalent continuum mechanics regions.

5 Interfacial Conditions between Atomistic Simulation (MD) Region and the Equivalent Continuum Mechanics (ECM) Region

In the multiscale simulation, the atomistic method is employed where the displacement field varies on an atomic scale, and the continuum approach is employed elsewhere. For the seamless multiscale simulation, it is important to ensure that the elastic waves generated in the atomistic region can propagate into the continuum region. The continuum region cannot support modes of short wavelength, which is less than the spacing of the nodes. One source of finite size effects is the short waves which are reflected back unphysically from an artificial interface or boundary, which may also produce uneven heating across the interface. In order to minimize such reflections, some interfacial conditions are proposed [Cai et al. (2000), E and Huang (2001), Wagner and Liu (2003)]. In this paper, alternate interfacial conditions between atomistic and continuum regions are proposed. Their effectiveness in ensuring the accurate passage of information between atomistic and continuum regions is discussed.

As mentioned before, the displacement $\mathbf{u}_i$ of an atom in region B [ECM] implies an average value of the atomic displacement, it can not catch the thermal fluctuations. To describe it more accurately, we assume that the "real" displacement $\mathbf{q}_i$ of the atom in the region B can be expressed as:

$$\mathbf{q}_i = \mathbf{u}_i + \delta \mathbf{u}_i \tag{65}$$

where $\delta \mathbf{u}_i$ denote the atomic thermal fluctuations, and it is assumed that $\delta \mathbf{u}_i << \mathbf{u}_i$ in region B. Now, the total potential energy of the system (A+B) [wherein Region A is of MD] can be written as:

$$\begin{aligned} \Pi(\mathbf{q}_1, \cdots, \mathbf{q}_{N_1+N_2}) &\approx \Pi(\mathbf{u}_i; \mathbf{q}_I) + \sum_{i=1}^{N_2} \left. \frac{\partial \Pi}{\partial \mathbf{q}_i} \right|_{\mathbf{q}_i = \mathbf{u}_i} \delta \mathbf{u}_i \\ &= \Pi_0 + \sum_{i=1}^{N_2} \frac{\partial \Pi_0}{\partial \mathbf{u}_i} \delta \mathbf{u}_i = \Pi_0(\mathbf{u}_B; \mathbf{q}_A) + \frac{\partial \Pi_0}{\partial \mathbf{u}_B} \cdot \delta \mathbf{u}_B \end{aligned} \tag{66}$$

($I = 1, \cdots, N_1$ in A; $i = 1, \cdots, N_2$ in B)

Here Π_0 denotes the zeroth-order approximation of the potential energy; $\mathbf{q}_A$ and $\mathbf{u}_B$ are the atomic displacement vectors with dimensions $3N_1$ (for 3 dimensions) in region A, and $3N_2$ in region B, respectively; $\delta \mathbf{u}_B$ is atomic thermal fluctuation vector with dimension $3N_2$. We can also expand the potential energy to a higher order, which will be at the expense of an additional computational cost. However, in the region B, the deformation is homogeneous, and $\delta \mathbf{u}_i$ is very small compared to $\mathbf{u}_i$, so that equation (66) is accurate enough. Effectively, the MLPG algorithm involves an average over the atomic degrees of freedom that are missing from the nodes in region B. The second term in right side of equation (66) accounts for the missing degrees of atomic freedom.

In many of the existing multiscale modeling methods, the thermal fluctuation is generally neglected, as in Rudd and Broughton (1998), Shenoy (2003), Abraham (2000). In this case, in region A, the Newton's Second law can be written in a matrix form as

$$\mathbf{M}_A \ddot{\mathbf{q}}_A = \mathbf{f}_A^0; \quad \mathbf{f}_A^0 = -\partial \Pi_0 / \partial \mathbf{q}_A \tag{67}$$

where the atomic mass matrix $\mathbf{M}_A$ is a diagonal matrix of size $3N_1$ with the atomic masses on the diagonal, and

the force vector $\mathbf{f}_A^0$ is of dimension $3N_1$. Eq. (67) is valid only for classical 0°K. We denote the solution of eq. (67) as "Solution Method 1". The degrees of freedom (DOF) N_1 in A are in general greater than these in B, viz., N_2 [i.e., $N_1 >> N_2$]. Thus, in Solution Method 1, which is computationally inexpensive, has the potential drawback that higher frequencies waves will reflect back from the interface between A and B.

To improve the performance at higher frequencies and assure that the energy in region A can pass through the interface between A and B, the thermal fluctuation of atoms in region B must be considered. Thus, we will use the first-order approximation of the potential energy, i.e. Π in eq. (66), to replace Π_0 in eq. (67), which leads to:

$$\mathbf{M}_A\ddot{\mathbf{q}}_A = \mathbf{f}_A^0 - \mathbf{K}_{AB}\delta\mathbf{u}_B \tag{68}$$

where

$$\mathbf{K}_{AB} = \partial^2\Pi_0/\partial\mathbf{u}_B\partial\mathbf{q}_A.$$

It is noted that the tangent stiffness matrix $\mathbf{K}_{AB}$ is of order $3N_1 \times 3N_2$, and its entries are nonzero, only when the atoms in region A are directly coupled to atoms in region B. $\delta\mathbf{u}_B$ can be obtained from the equation of motion in region B, viz.,

$$\mathbf{M}_B\delta\ddot{\mathbf{u}}_B = \mathbf{f}_B^0 - \mathbf{M}_B\ddot{\mathbf{u}}_B \tag{69}$$

where the atomic mass matrix $\mathbf{M}_B$ is a diagonal matrix of size $3N_2$, and the force vector $\mathbf{f}_B^0$ of dimension $3N_2$ is approximated as

$$\mathbf{f}_B^0 = -\partial\Pi_0/\partial\mathbf{u}_B \tag{70}$$

In equations (68) and (69), we note that $\mathbf{f}_A$ *in region A is approximated as* $\mathbf{f}_A = -\partial\Pi/\partial\mathbf{q}_A \approx -\partial\Pi_0/\partial\mathbf{q}_A - \partial^2\Pi_0/\partial\mathbf{u}_B\partial\mathbf{q}_A\delta\mathbf{u}_B$; *that in region B is approximated as* $\mathbf{f}_B = -\partial\Pi/\partial\mathbf{q}_B$. By integrating eq. (69) twice, $\delta\mathbf{u}_B$ can be solved for, and substituting this solution into eq. (68), we have

$$\mathbf{M}_A\ddot{\mathbf{q}}_A = \mathbf{f}_A^0(\mathbf{u}_B,\mathbf{q}_A) - \mathbf{K}_{AB}\int_0^t (t-\tau)\,\mathbf{Y}(\tau)\,d\tau - \mathbf{R}(t) \tag{71}$$

where

$$\mathbf{Y}(t) = \mathbf{M}_B^{-1}\mathbf{f}_B^0(\mathbf{u}_B,\mathbf{q}_A) - \ddot{\mathbf{u}}_B(t) \tag{72}$$

$$\mathbf{R}(t) = \mathbf{K}_{AB}\left[\delta\mathbf{u}_B(0) + t\delta\dot{\mathbf{u}}_B(0)\right] \tag{73}$$

$\mathbf{Y}(t)$ simply represents $\delta\ddot{\mathbf{u}}_B$. $\mathbf{R}(t)$ represents the effects on region A due to the initial thermal fluctuation, and the velocity in region B and is usually treated as a vector of random forces to describe the effects of statistical fluctuation in region B at nonzero temperature. In the example problems in section 7, it is assumed that the temperature is 0°K, so that $\mathbf{R}(t)$ can be ignored. The solution of eq. (71), which is originally proposed here, is denoted as "Solution Method 2". It is noted that only a few of the entries in vector $\mathbf{Y}(t)$ are necessary, since the matrix $\mathbf{K}_{AB}$ is nonzero only for the atomic pairs in the cutoff of the interface. That makes presently proposed Solution Method 2 is computationally inexpensive.

Now, we will give a brief discussion about the second term on the right hand side of equation (71). Assuming that the time step is Δt, and all the quantities are obtained at the ith time step, then at the (i+1)th time step, we have

$$\begin{aligned}
\mathbf{J}_{i+1} &= \int_0^{t_{i+1}} (t_{i+1}-\tau)\,\mathbf{Y}(\tau)\,d\tau \\
&= t_{i+1}\int_0^{t_{i+1}} \mathbf{Y}(\tau)\,d\tau - \int_0^{t_{i+1}} \tau\mathbf{Y}(\tau)\,d\tau \\
&= t_{i+1}\int_0^{t_i} \mathbf{Y}(\tau)\,d\tau + t_{i+1}\int_{t_i}^{t_{i+1}} \mathbf{Y}(\tau)\,d\tau - \int_0^{t_i} \tau\mathbf{Y}(\tau)\,d\tau \\
&\quad - \int_{t_i}^{t_{i+1}} \tau\mathbf{Y}(\tau)\,d\tau \\
&= t_{i+1}\hat{\mathbf{Y}}_i + t_{i+1}\int_{t_i}^{t_{i+1}} \mathbf{Y}(\tau)\,d\tau - \tilde{\mathbf{Y}}_i - \int_{t_i}^{t_{i+1}} \tau\mathbf{Y}(\tau)\,d\tau \\
&= \left(t_i\hat{\mathbf{Y}}_i - \tilde{\mathbf{Y}}_i\right) + \Delta t\hat{\mathbf{Y}}_i + t_{i+1}\int_{t_i}^{t_{i+1}} \mathbf{Y}(\tau)\,d\tau - \int_{t_i}^{t_{i+1}} \tau\mathbf{Y}(\tau)\,d\tau \\
&= \mathbf{J}_i + \Delta t\hat{\mathbf{Y}}_i + t_{i+1}\Delta\hat{\mathbf{Y}} - \Delta\tilde{\mathbf{Y}} = \mathbf{J}_i + t_i\Delta\hat{\mathbf{Y}} - \Delta\tilde{\mathbf{Y}} \\
&\quad + \left(\Delta t\hat{\mathbf{Y}}_i + \Delta\hat{\mathbf{Y}}\right) \\
&= \mathbf{J}_i + t_i\Delta\hat{\mathbf{Y}} - \Delta\tilde{\mathbf{Y}} + \Delta t\hat{\mathbf{Y}}_{i+1}
\end{aligned}$$

with

$$\hat{\mathbf{Y}}_i = \int_0^{t_i} \mathbf{Y}(\tau)\,d\tau$$

$$\hat{\mathbf{Y}}_{i+1} = \hat{\mathbf{Y}}_i + \Delta\hat{\mathbf{Y}}$$

$$t_{i+1} = t_i + \Delta t$$

and

$$\Delta\hat{\mathbf{Y}} = \int_{t_i}^{t_{i+1}} \mathbf{Y}(\tau)\,d\tau = \frac{\Delta t}{2}\left[\mathbf{Y}(t_i) + \mathbf{Y}(t_{i+1})\right]$$

$$\Delta\tilde{\mathbf{Y}} = \int_{t_i}^{t_{i+1}} \tau\mathbf{Y}(\tau)\,d\tau = \frac{\Delta t}{2}\left[t_i\mathbf{Y}(t_i) + t_{i+1}\mathbf{Y}(t_{i+1})\right]$$

From the above equations, it can be seen that they only used the results at the ith and the (i+1)th time steps, to calculate the second term on the right hand side of equation (71) [only the entries for the atomic pairs in the cutoff of the interface are needed] at (i+1) time step. Hence, a complete time history of the trajectory is not needed to evaluate the second term on the right hand side of equation (71).

In equations (68) and (69), which are based on the potential energy, we note that the force in the region A is expanded to the first order of $\delta\mathbf{u}_B$, while the force in the region B is only of the zeroth order. To increase the accuracy of the results, we can also expand the force in the region B to the first order, as

$$\mathbf{f}_B = \mathbf{f}_B^0 + \mathbf{K}_{BB}\delta\mathbf{u}_B \tag{74}$$

with the $3N_2 \times 3N_2$ tangent stiffness matrix

$$\mathbf{K}_{BB} = \partial^2\Pi_0/\partial\mathbf{u}_B\partial\mathbf{u}_B$$

Then, eq. (69) can be rewritten as

$$\mathbf{M}_B\delta\ddot{\mathbf{u}}_B = \mathbf{f}_B^0 + \mathbf{K}_{BB}\delta\mathbf{u}_B - \mathbf{M}_B\ddot{\mathbf{u}}_B \tag{75}$$

Similar to Adelman and Doll (1976), by means of Laplace transforms, the intermediate-variable $\delta\mathbf{u}_B$ can be solved for, and substituting it back into eq. (68), we have

$$\mathbf{M}_A\ddot{\mathbf{q}}_A = \mathbf{f}_A^0(\mathbf{u}_B, \mathbf{q}_A) - \int_0^t \boldsymbol{\vartheta}(t-\tau)\,\mathbf{Y}(\tau)\,d\tau + \mathbf{R}(t) \tag{76}$$

where

$$\boldsymbol{\vartheta}(t) = L^{-1}\left\{\mathbf{K}_{AB}\left[s^2\mathbf{I} + \mathbf{M}_B^{-1}\mathbf{K}_{BB}\right]^{-1}\right\} \tag{77}$$

$$\mathbf{R}(t) = \dot{\boldsymbol{\vartheta}}(t)\delta\mathbf{u}_B(0) + \boldsymbol{\vartheta}(t)\delta\dot{\mathbf{u}}_B(0) \tag{78}$$

The matrix $\boldsymbol{\vartheta}(t)$ denotes the time-dependent memory kernel. The Operator L^{-1} indicates the inverse Laplace transform. Eq. (76) is similar to the Generalized Langevin Equation (GLE) boundary condition derived in Adelman and Doll (1976) for the single-scale problem, and in Wagner and Liu (2003) for the multiscale problem by using a "bridging scale" decomposition [i.e., the entire system is treated as a coarse scale one, B, first; and then the entire system is treated as a fine scale one, A, later sequentially. In the present paper, the system is treated as a combination of parts A and B simultaneously]. We denote the solution of eq. (75) as "Solution Method 3".

The second term on the right hand side of equations (71) and (75), the time history integral, implies the dissipation of energy from region A into region B, which results in non-reflecting boundary conditions, supporting short wavelengths that cannot be represented by the interpolations in region B.

It is noted that the computation of the of the matrix $\boldsymbol{\vartheta}(t)$ involves not only an inverse Laplace transform, but also the inversion of an $N_2 \times N_2$ matrix, which appears to be impractical, although only a few of the entries in this inverted matrix are necessary, since the matrix $\mathbf{K}_{AB}$ is nonzero only for atomic pairs in the cutoff of the interface. The necessary entries of the matrix $\boldsymbol{\vartheta}(t)$ can be approximated as that in Adelman and Doll (1976), or computed numerically as in Cai at al. (2000). However, the computation of the matrix $\boldsymbol{\vartheta}(t)$ is costly. Moreover, a complete time history of the trajectory is required to evaluate the second term on the right hand side of equation (76). In our numerical examples, we will not consider Solution Method 3.

6 Multiple Time Steps for Time Integration

In this paper, a multiple time step method is employed for the time integration in both region A and B. The stability of multiple time step method was studied in Belytschko et al. (1979), Belytschko and Smolinski (1985), Belytschko and Lu (1993). The standard method would be to use the central difference rule. In region B, the time step is taken to be Δt_B. In region A, the time step is $\Delta t_A = \Delta t_B/k$, where k is a positive integer and determined by the spacing of the nodes. Hence, the MD simulation in region A is advanced by k steps of size Δt_A, when the ECM simulation in region B is advanced for a step of size Δt_B.

The scheme for time integration in region A from time step $nk+i$ to $nk+i+1$ is as follows:

$$\mathbf{d}^{nk+i+1} = \mathbf{d}^{nk+i} + \Delta t_A\dot{\mathbf{d}}^{nk+i} + \frac{1}{2}\Delta t_A^2\ddot{\mathbf{d}}^{nk} \tag{79}$$

$$\dot{\mathbf{d}}^{nk+i+1} = \dot{\mathbf{d}}^{nk+i} + \Delta t_A\ddot{\mathbf{d}}^{nk} \tag{80}$$

Then, the displacements $\mathbf{u}_B^{nk+i+1}$, of atom in the cutoff of the interface, in region B are interpolated by equation (30), and then

$$\mathbf{q}_A^{nk+i+1} = \mathbf{q}_A^{nk+i} + \Delta t_A\dot{\mathbf{q}}_A^{nk+i} + \frac{1}{2}\Delta t_A^2\ddot{\mathbf{q}}_A^{nk+i} \tag{81}$$

$$\ddot{\mathbf{q}}_A^{nk+i+1} = \mathbf{M}_A^{-1}\mathbf{f}_A^R\left(\mathbf{u}_B^{nk+i+1}, \mathbf{q}_A^{nk+i+1}\right) \tag{82}$$

$$\dot{\mathbf{q}}_A^{nk+i+1} = \dot{\mathbf{q}}_A^{nk+i} + \frac{1}{2}\Delta t_A\left(\ddot{\mathbf{q}}_A^{nk+i+1} + \ddot{\mathbf{q}}_A^{nk+i}\right) \tag{83}$$

where $0 \le i < k$, $\mathbf{f}_A^R\left(\mathbf{u}_B^{nk+i+1}, \mathbf{q}_A^{nk+i+1}\right)$ represents the entire right hand side of equation (67) or (71) or (76). It is noted that in equations (79) and (80), only the quantities in the cutoff of the interface are needed. For all the k steps from step nk, the acceleration of the nodes in region B is assumed to be constant.

Once $\mathbf{q}_A^{(n+1)k}$ are obtained at $(n+1)k$ time step, the node-displacement in region B is advanced form time step nk to $(n+1)k$. The scheme for time integration in region B from time step nk to $(n+1)k$ is as follows

$$\mathbf{d}^{(n+1)k} = \mathbf{d}^{nk} + \Delta t_B\dot{\mathbf{d}}^{nk} + \frac{1}{2}\Delta t_B^2\ddot{\mathbf{d}}^{nk} \tag{84}$$

$$\ddot{\mathbf{d}}^{(n+1)k} = \mathbf{M}_C^{-1}\mathbf{t}_C\left(\mathbf{d}^{(n+1)k}, \mathbf{q}_A^{(n+1)k}\right) \tag{85}$$

$$\dot{\mathbf{d}}^{(n+1)k} = \dot{\mathbf{d}}^{nk} + \frac{1}{2}\Delta t_B\left(\ddot{\mathbf{d}}^{nk} + \ddot{\mathbf{d}}^{(n+1)k}\right) \tag{86}$$

It is noted that equations (79) and (80) give the same node-displacement at $(n+1)k$ time step as equation (84). Once these quantities at $(n+1)k$ time step are determined, they will be used in equations (79) and (80).

7 Numerical Examples

7.1 one-dimensional chains

As a demonstration of the effectiveness of the multiscale simulation method and the interfacial conditions proposed here, we consider the same example as in Rudd and Broughton (1998), Cai, et al. (2000), and Wagner and Liu (2003): one-dimensional chains of identical atoms with nearest-neighbor interactions. The spring constants, mass, and equilibrium distances are set equal to unity. There are 151 atoms in region A, which is bracketed by two semi-infinite chains (region B). The lumped mass matrix is used. The time integration uses multiple time steps: the equivalent continuum simulation in region B is advanced by a time step $\Delta t_B = 0.1$, while the MD simulation in region A is advanced by $\Delta t_A = \Delta t_B/5$. The distance between the nodes in region B is h=7.8. The radius of the trial function domain is taken to be $3.2h$, and the radius of the test domain is $0.85h$. The Solution Methods denoted as 1 and 2 earlier, are used to simulate the time evolution, after introducing initial displacements according to the wave packet [Rudd and Broughton (1998), Cai, et al. (2000)]:

$$u(X, t=0) = \cos(kX)\exp\left(-X^2/2\sigma^2\right) \tag{87}$$

Here, X denotes the equilibrium position of atoms. The center of region A is $X = 0$. A full MD simulation is also performed, in which the entire system is treated in an atomistic scale. As a measure of the effectiveness of Solution Methods 1 and 2, the wave reflection at the interface between region A and B is evaluated. The reflectivity R is defined as the maximum difference between the instantaneous energies stored in region A during the simulation and the full MD run, divided by initial energy in region A [Cai, et al. (2000)].

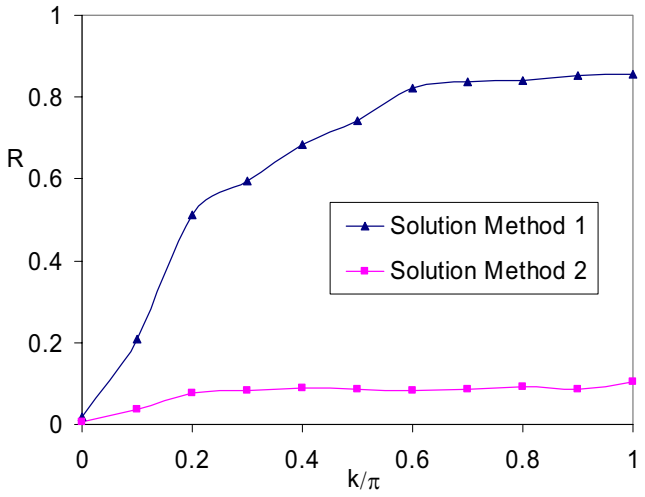

Figure 4 : Comparison of the phonon reflectivity R in two solution methods.

Fig. 4 shows the variation of phonon reflectivity R versus the wave number k with $\sigma = 5$. In both cases shown, R approaches to zero in the long wave-length limit. As the wave number increases, R increases greatly, and is over 0.8 at the boundary of Brillouin zone in Solution Method 1, while it is less than 0.1 in all the Brillouin zone in Solution Method 2. Solution Method 1 obtains lower R than that in Rudd and Broughton (1998), and Abraham (2000), that means MLPG will be a better method for a seamless multiscale simulation than the finite element

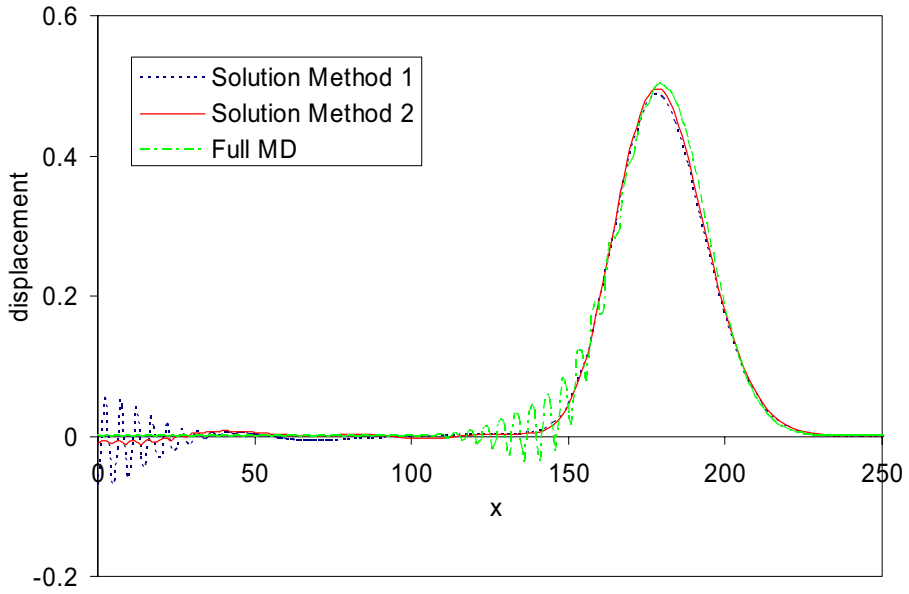

Figure 5 : Comparison of the displacement profiles computed using the multiscale methods and the full MD, at t=18.

method. However, Solution Method 1 is much less effective than the Solution Method 2. Although lower R can be reached in the Solution Method 3 [Cai, et al. (2000)], due to its high computational cost, Solution Method 3 should not be an appropriate choice among the three solutions in most problems.

Another example is the same problem as in Wagner and Liu (2003). A short wave-length perturbation is multiplied to a Gaussian pulse. The resulting initial displacement is

$$u(X,t=0)=\frac{\left[\exp\left(-X^2/\sigma^2\right)-u_c\right]}{1-u_c}\left[1+0.1\cos\left(kX\right)\right] \tag{88}$$

Here, $u_c=\exp\left(-l^2/\sigma^2\right)$, $l=50$, $\sigma=20$, $k=0.4\pi$. All the other parameters are same as in the first example. Fig. 5 shows the displacements obtained by Solution Methods 1 and 2, and full MD at $t=18$. Because of the configurational symmetry about $X=0$, only the right plane is plotted. An internal reflection of the short wave-length perturbation appears in Solution Method 1, which looks like the mirror image of the short wave-length perturbation in full MD with the mirror located on the interface of region A and B ($X=75$). In Solution Method 2, the short wave-length waves almost pass out of region A at the same time as the long wave-length Gaussian pulse propagates into region B. In region B, both cases simulate the long wave-length Gaussian wave very well. Compared with the full MD solution, there is an apparent smoothing of the wave profile as the Gaussian pulse propagates in region B, due to the large node space.

To make sure that the mass-lumping procedure (55)-(56) are correct, we also used the consistent mass matrix in Solution Method 2 in this example. The results show that both the lumped and consistent mass work very well. A Comparison of the displacement profiles computed using the consistent and lumped mass in Solution Method 2, at t=18 is plotted in Fig. 6. The initial displacement profile is also plotted in Fig. 6.

7.2 Two-dimensional grapheme sheet

This multiscale method can be generalized to multiaxial problems. In this subsection, a planar problem is considered to demonstrate the method without loss of generality. The formulations can be extended to more complicated 3-D systems. The problem is of a graphene sheet of one-atom thickness.

In this example, the Tersoff-Brenner potential [Tersoff (1988), Brenner (1990)] is used for the energy associated with the deformation of the atoms. It is given as a sum

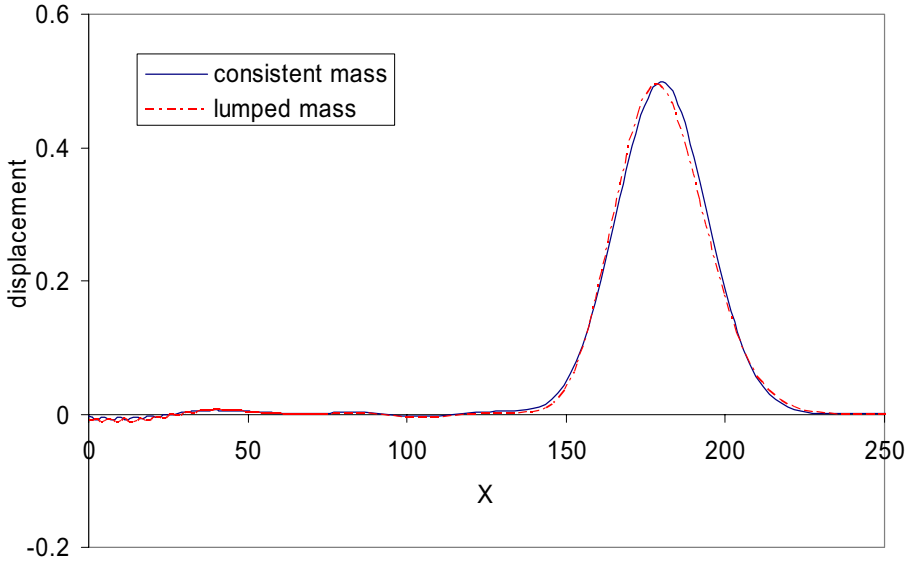

Figure 6 : Comparison of the displacement profiles computed using the consistent and lumped mass in Solution Method 2, at t=18, and the initial displacement profile.

over bonds as

$$\Pi = \sum_{I} \sum_{J(>I)} \left[V_R(r_{IJ}) - \overline{B} V_A(r_{IJ}) \right] \tag{89}$$

which has repulsive and attractive terms, respectively,

$$V_R(r_{IJ}) = \frac{f_{IJ}(r) D^{(e)}}{(S-1)} e^{-\sqrt{2S}\beta\left(r-R^{(e)}\right)} \tag{90}$$

$$V_A(r_{IJ}) = \frac{f_{IJ}(r) D^{(e)} S}{(S-1)} e^{-\sqrt{\frac{2}{S}}\beta\left(r-R^{(e)}\right)} \tag{91}$$

with the functions of the bond angle

$$\overline{B} = \frac{1}{2}\left(B_{IJ} + B_{JI}\right) \tag{92}$$

$$B_{IJ} = \left[1 + \sum_{K(\neq I,J)} G(\theta_{IJK}) f_{IK}(r_{IK}) \right]^{-\delta} \tag{93}$$

$$G(\theta) = a_0 \left\{ 1 + \frac{c_0^2}{d_0^2} - \frac{c_0^2}{d_0^2 + (1+\cos\theta)^2} \right\} \tag{94}$$

and the cut-off function which limits the rang of the interactions

$$f_{IJ}(r) = \begin{cases} 1, & r < R^{(1)} \\ \frac{1}{2} + \frac{1}{2}\cos\left[\frac{\pi\left(r-R^{(1)}\right)}{\left(R^{(2)}-R^{(1)}\right)} \right], & R^{(1)} < r < R^{(2)} \\ 0, & r > R^{(2)} \end{cases}$$

(95)

where the constants for carbon are

$$R^{(e)} = 1.39\text{Å}, \quad D^{(e)} = 6.0 \text{ eV}, \quad S = 1.22,$$
$$\beta = 2.1\text{Å}^{-1}, \quad \delta = 0.5, R^{(1)} = 1.7\text{Å}, \quad R^{(2)} = 2.0\text{Å},$$
$$a_0 = 2.0813 \times 10^{-4}, \quad c_0 = 330, \quad d_0 = 3.5$$

and the mass of the carbon atom is $m_I = 12.01115 \times 1.65979 \times 10^{-27}$ kg, and 1 ev $= 1.602 \times 10^{-19}$ J.

As discussed in section 3, in this method, the energy will be written in a form that is additively decomposed. Hence, equation (89) will be rewritten as sum over atomic site I,

$$\Pi = \sum_{I=1} \Pi_I \tag{96}$$

where each contribution Π_I is written as

$$\Pi_I = \frac{1}{2} \sum_{J(\neq I)} \left[V_R(r_{IJ}) - B_{IJ} V_A(r_{IJ}) \right] \tag{97}$$

Then, the stress in equation (53) can be written as

$$\begin{aligned}\frac{\partial W}{\partial \mathbf{F}} &= \frac{1}{\Delta\Omega_I}\frac{\partial \Pi_I}{\partial \mathbf{F}} \\ &= \frac{1}{2\Delta\Omega_I}\sum_{J(\neq I)}\left[V_R'\frac{\partial r_{IJ}}{\partial \mathbf{r}_{IJ}} - V_A\frac{\partial B_{IJ}}{\partial \mathbf{r}_{IJ}} - B_{IJ}V_A'\frac{\partial r_{IJ}}{\partial \mathbf{r}_{IJ}}\right]\otimes\frac{\partial \mathbf{r}_{IJ}}{\partial \mathbf{F}} \\ &\quad + \frac{1}{2\Delta\Omega_I}\sum_{J(\neq I)}\left[-V_A\frac{\partial B_{IJ}}{\partial \mathbf{r}_{IK}}\otimes\frac{\partial \mathbf{r}_{IK}}{\partial \mathbf{F}}\right] \end{aligned} \tag{98}$$

and the force on the atom I can be obtained as

$$\begin{aligned}\mathbf{f}_I &= -\frac{\partial \Pi}{\partial \mathbf{x}_I} = -\frac{\partial \Pi}{\partial \mathbf{q}_I} \\ &= \frac{1}{2}\sum_{J(\neq I)}\left[-V_R'\frac{\partial r_{IJ}}{\partial \mathbf{r}_{IJ}} + V_A\frac{\partial \overline{B}_{IJ}}{\partial \mathbf{r}_{IJ}} + \overline{B}_{IJ}V_A'\frac{\partial r_{IJ}}{\partial \mathbf{r}_{IJ}}\right] \\ &\quad + \frac{1}{2}\sum_{J(\neq I)}\sum_{K(\neq I,J)}\left[-V_A(r_{JK})\frac{\partial B_{JK}}{\partial \mathbf{r}_{JI}}\right] \end{aligned} \tag{99}$$

The example is that of a 2D graphene sheet of one-atom thickness, with 452.2764 Å length, 68.1819 Å width, which has 11,552 atoms. The thickness of the sheet is taken to be 3.4 Å, which is the standard layer separation thickness for graphite. At the equilibrium sate, which is taken to be the reference frame, the nearest neighbor bond length is b=1.4507 Å. The sheet is fixed at left and right edges. Periodic boundary conditions in the direction parallel to the surface are imposed, thus the effects of the upper and lower surface are neglected. Initial displacements are introduced, according to the plane wave packet

$$\begin{aligned}&u_1(X_1,X_2,t=0) \\ &= \frac{\left[\exp\left(-X_1^2/\sigma^2\right)-u_c\right]}{1-u_c}\left[1+0.1\cos\left(\frac{kX_1}{a}\right)\right] \\ &u_2(X_1,X_2,t=0)=0 \end{aligned} \tag{100}$$

where $u_c=\exp\left(-l^2/\sigma^2\right)$, $l=40a$, $\sigma=15a$, $a=\sqrt{3}b/2$, $k=0.5\pi$. Here, X_1 and X_2 denote the positions of atoms in the reference frame, and u_1 and u_2 denote the displacement in the X_1 and X_2 direction, respectively. The center line of the sheet is $X_1=0$. Because of the configurational symmetry about $X_1=0$, only the right plane is considered in this numerical example. The computational domain is $[0,226.1382]\times[0,68.1819]$. The region A is $[0,74.1242]\times[0,68.1819]$; this region contains 1920 atoms. The region B containing 5792 atoms, is discretized into a set of nodes. Two sets of nodes are used in this paper, the coarse one includes 19×10 nodes, and the fine one includes 38×20 nodes. Fig. 6 is a part of the distribution of the atoms and nodes in the reference frame for the coarse one. The nodes in the region B are distributed evenly, although it is unnecessary. However, on the interface of region A and B, the nodes are taken to be the atoms, as show in Fig. 7. Actually, these nodes are only used for the interpolation, their motions is still governed by atomic motion equation (57).

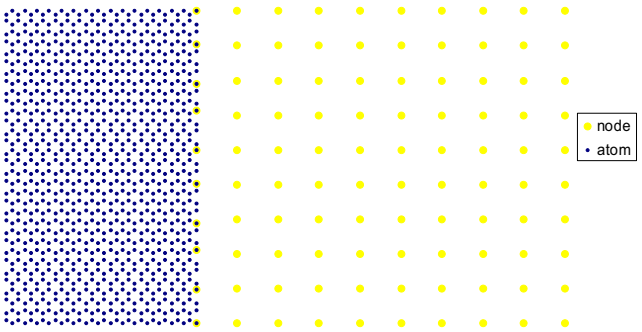

Figure 7 : The distribution of the atoms and nodes in the reference frame.

The computational setup described above is used to simulate the propagation of a plane wave packet (100). The equivalent continuum simulation in region B is advanced by a time step $\Delta t_B=5\times10^{-15}$s, while the MD simulation in region A is advanced by $\Delta t_A=\Delta t_B/10=5\times10^{-16}$s. The radius of the trial function domain in Region B is taken to be $4.2h$, where h represents the distance between the nodes in region B, and the radius of the test domain is $0.85h$. The Solution Method 2, with the lumped mass matrix, is used to simulate the time evolution. A full MD simulation is also performed to verify our numerical results.

Fig. 8 shows the displacement profiles of u_1 for the atoms along X_2=34.8168 Å at different moments by using the full MD simulation. The displacement u_2 should be 0 in this case. Fig. 9 and Fig. 10 are the corresponding displacement profiles obtained from the multiscale simulation by using the coarse and fine nodes, respectively.

Comparing Fig. 8 - Fig. 10, we can find that both coarse and fine cases can obtain good results. In Fig. 11, the comparison of the displacement profiles at t=0.5 ps from

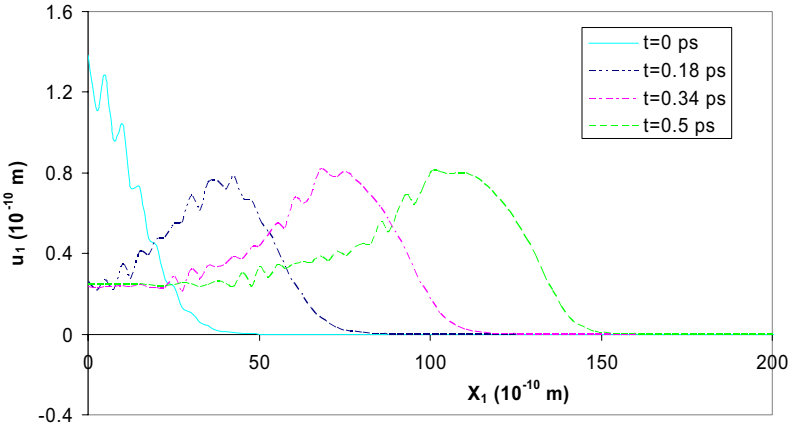

Figure 8 : The displacement profiles of u_1 along X_2=34.8168 Å at different moments (full MD)

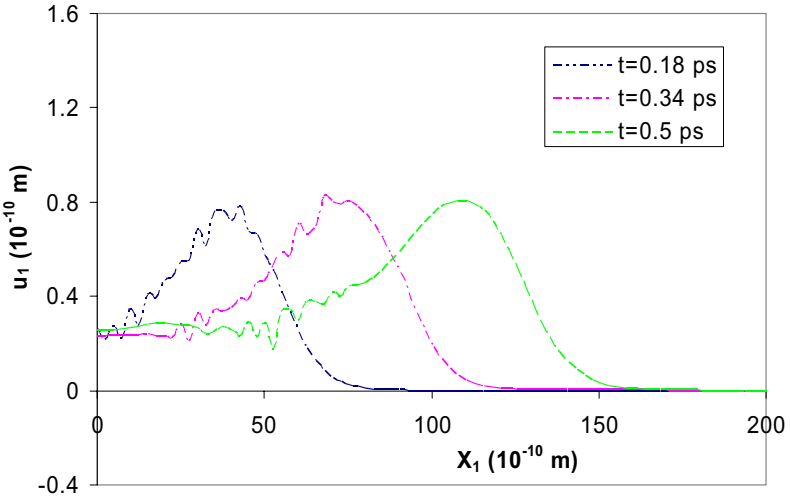

Figure 9 : The displacement profiles of u_1 along X_2=34.8168 Å at different moments (Coarse)

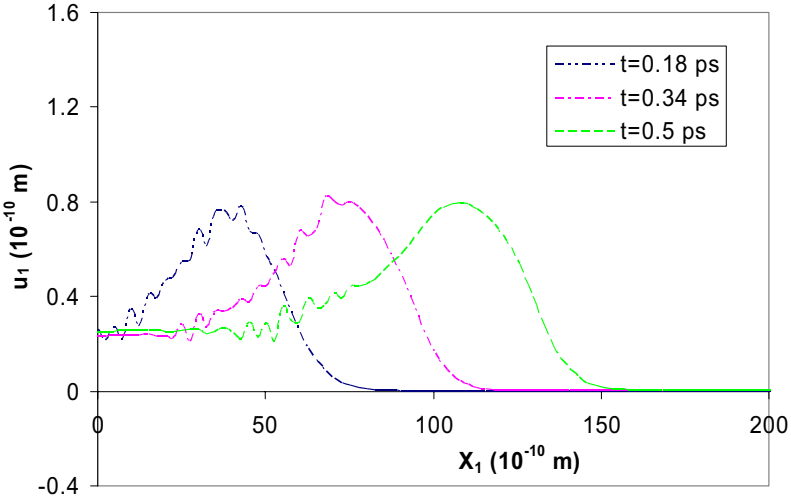

Figure 10 : The displacement profiles of u_1 along X_2=34.8168 Å at different moments (fine)

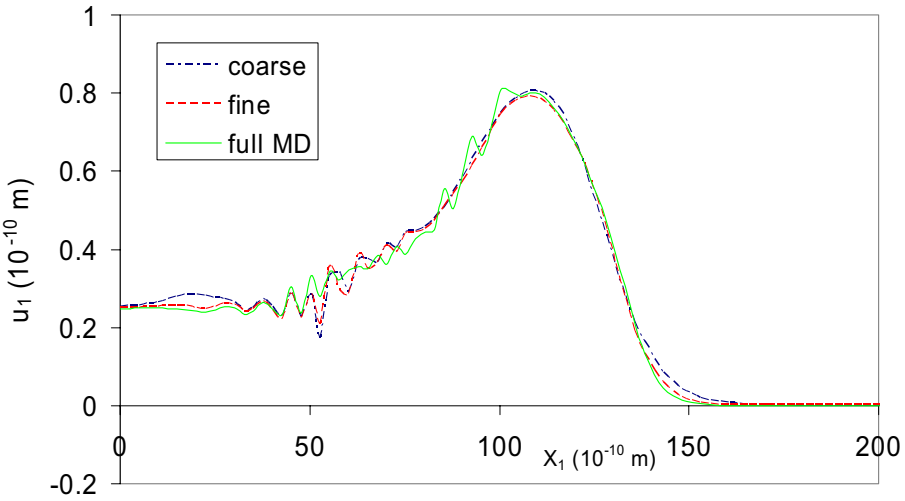

Figure 11 : Comparison of the displacement profiles of u_1 along X_2=34.8168 Å, computed using the multiscale methods and the full MD, at t=0.5 ps.

these 3 figures, are plotted. Compared with the full MD solution, there is an apparent smoothing of the wave profile as the wave propagates in region B, due to the large node spacing. Certainly, the fine one can get better results than the coarse one. We also choose two atoms, one in region A with coordinates (61.5608, 34.8186), another in region B with coordinates (87.6876, 34.8186), to compare their trajectories. The results are plotted in Fig. 12. Obviously, in region B, we can only obtain the average displacements of the atoms, the fluctuation cannot be captured. Hence, the trajectory of the atom in region B is smoothed, but it does not losse the essential characteristics of the trajectory. Fig. 13 is the displacement profile of the right half sheet at t=0.5 ps. The three coordinates in this figure are X_1, X_2, and u_1, respectively. This result was obtained by using the coarse space resolution.

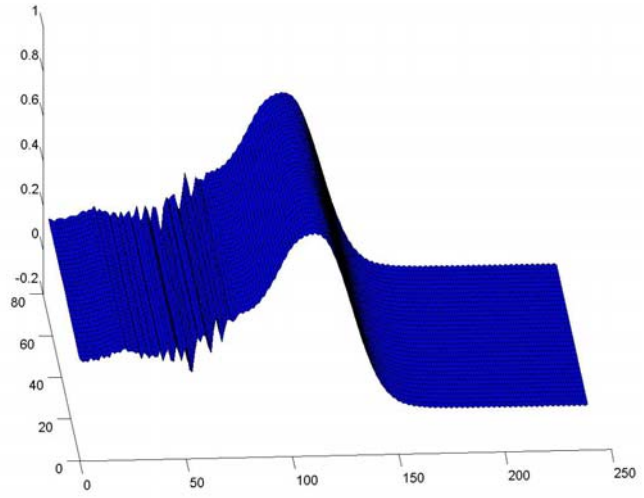

Figure 13 : The displacement profiles of u_1 at t=0.5 ps.

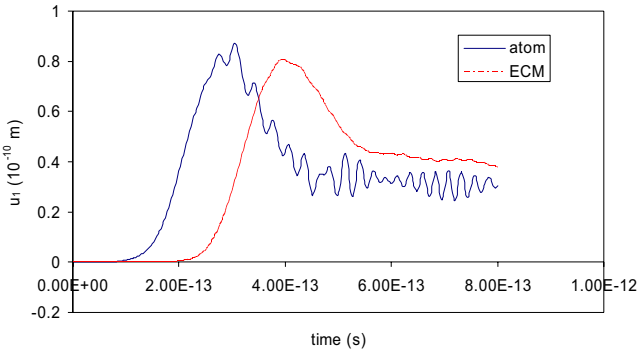

Figure 12 : The trajectories of two atoms

8 Conclusion

A multiscale simulation technique, based on a combination of MD and MLPG methods has been implemented and tested. Multiple length scale, multiple time steps technique are used in the numerical examples. Good agreement of wave profile in MD and ECM parts is observed in the simulation. Three alternate interfacial conditions are derived, for the multiscale simulation, by considering the fluctuation of atoms in the continuum region. Solution Method 2, proposed in this paper, is found to

be optimal in both reducing the reflection of phonons and in lowering computational cost, especially when the atomistic region moves with time, which is the case that intrigues us. The MLPG method is also found to be very effective in seamless multiscale simulations. In this method, a wave can be transported from the MD region to the ECM region without losing the essential characteristics of the wave profile.

This multiscale simulation method allows one to balance the level of details necessary to provide reasonable accuracy in some regions of the model, with computational cost. The applications of this methodology will be many and varied. This method will play a key role in the simulation and design methodology for nanodevices.

Acknowledgement: This work was supported by the U. S. Army Research Office, and the U. S. Army Research Laboratory, under a cooperative research agreement with the University of California at Irvine. The Cognizant Program Official at the U. S. Army Research Labs is Dr. R. Namburu. Partial support for this work was also provided by the Office of Naval Research, in the program directed by Dr. Y.D.S. Rajapakse.

References

Abraham, F. F. (2000): MAADLY spanning the length scales in dynamic fracture. *CMES: Computer Modeling in Engineering & Sciences* 1(4): 63-69

Adelman, S. A.; Doll, J. D. (1976): Generalized Langevin equation approach for atom-solid-surface scattering –general formulation for classical scattering off harmonic solids. *J. Chem. Phys.* 64: 2375-2388.

Ajayan, P. M.; Zhou, O. Z. (2001): " Applications of Carbon Nanotubes", in *Carbon Nanotubes*, Topics in Applied Physics; M.S. Dresselhaus, et al (Eds); 80, 391-425, Springer

Arroyo, M.; Belytschko, T. (2002): An atomistic based finite deformation membrance for crystalline films one atom thick. *Journal of the Mechanics and Physics of Solids* 50(9): 1941-1977

Atluri, S. N. (1979): On rate principles for finite strain analysis of elastic and inelastic nonlinear solids. In *Recent Research on Mechanical Behavior*, 79-107, University of Tokyo Press.

Atluri, S. N. (1980): On some new general and complementary energy theorems for the rate problems in finite strain, classical elastoplasticity. *Journal of Structural Mechanics* 8(1): 61-92.

Atluri, S. N. (2004): *The meshless local Petrov-Galerkin (MLPG) method for domain and boundary discretization*. Tech. Science Press (in press).

Atluri, S. N.; Zhu, T. (1998): A new meshless local Petrov-Galerkin (MLPG) approach in computati**A**onal mechanics. *Comput. Mech*. 22: 117-127.

Atluri, S. N.; Shen, S. (2002a): *The meshless local Petrov-Galerkin (MLPG) method*. Tech. Science Press, 440 pages.

Atluri, S. N.; Shen, S. (2002b): The meshless local Petrov-Galerkin (MLPG) method: A simple & less-costly alternative to the finite element and boundary element method. *CMES: Computer Modeling in Engineering & Sciences* 3(1): 11-52

Atluri, S. N.; Shen, S. (2004): The Basis of Meshless Domain Discretization: The Meshless Local Petrov Galerkin (MLPG) Method. *Advances in Computational Mathematics* (in press)

Atluri, S. N.; Han, Z. D.; Shen, S. (2003): Meshless Local Patrov-Galerkin (MLPG) approaches for weakly-singular traction & displacement boundary integral equations, *CMES: Computer Modeling in Engineering & Sciences* 4(5): 507-516.

Batra, R. C.; Ching, H. K. (2002): Analysis of elastodynamic deformations near a crack/notch tip by the meshless local Petrov-Galerkin (MLPG) method. *CMES: Computer Modeling in Engineering & Sciences* 3(6): 717-730.

Belytschko, T.; Smolinski, P.; Liu, W. K. (1985): Stability of multi-time step partitioned integrators for 1st-order finite-element systems. *Comput. Meth. Appl. Mech. Eng.* 49: 281-297.

Belytschko, T.; Lu, Y. Y. (1993): Explicit multi-time step integration for 1st and 2nd-order finite-element semidiscretizations. *Comput. Meth. Appl. Mech. Eng.* 108: 353-383.

Belytschko, T.; Yen, H.; Mullen, R. (1979): Mixed methods for time integration. *Comput. Meth. Appl. Mech. Eng.* 17-8: 258-275.

Born, M.; Huang, K. (1954): Dynamical theory of crystal lattices. Oxford: Clarendon Press.

Brenner, D. W. (1990): Empirical potential for hydrocarbons for use in simulating the chemical vapor deposi-

tion of diamond films. *Phys. Rev*. B 42(15): 9458-9471.

Cai, W.; de Koning, M.; Bulatov, V. V.; Yip, S. (2000): Minimizing boundary reflections in coupled-domain simulations. *Phys. Rev. Lett*. 85: 3213-3216.

Chung, P. W.; Namburu, R. R.; Henz, B. J. (2004): A Lattice Statics Based Tangent Stiffness Finite Element Method, *CMES: Computer Modeling in Engineering & Sciences* 5(1): 45-62.

Cousins, C. S. G. (1978): Inner elasticity. *J. Phys. C: Solid State Phys*. 11: 4867-4879.

E, W.; Huang, Z. (2001): Matching conditions in atomistic-continuum modeling of materials. *Phys. Rev. Lett*. 87, art. No.-135501.

Ericksen, J. L. (1984): *Phase transformations and material instabilities in solids*. Academic Press: 61-77.

Ghoniem, N. M.; Cho, K. (2002): The emerging role of multiscale modeling in nano and micro-mechanics of materials. *CMES: Computer Modeling in Engineering & Sciences* 3(2): 147-173.

Han, Z. D.; Atluri, S. N. (2003): On Simple Formulations of Weakly-Singular Traction & Displacement BIE, and Their Solutions through Petrov-Galerkin Approaches. *CMES: Computer Modeling in Engineering & Sciences* 4(1): 5-20

Hardy, R. L. (1971): Multiquadric equations of topography and other irregular surfaces. *J. Geophys. Res*. 76: 1905-1915.

Li, Q.; Shen, S.; Han, Z. D.; Atluri, S. N. (2003): Application of Meshless Local Petrov-Galerkin (MLPG) to Problems with Singularities, and Material Discontinuities, in 3-D Elasticity, *CMES: Computer Modeling in Engineering & Sciences* 4(5): 567-581.

Liu, G. R.; Gu, Y. T. (2001): A local radial point interpolation method for free vibration analysis of 2D solids. *J. Sound Vibration* 246: 29-46.

Martin, J. W. (1975): Many-body forces in solids and the Brugger elastic constants: II. Inner elastic constants. *J. Phys. C: Solid State Phys*. 8: 2858-2868.

Rudd, R. E.; Broughton, J. Q. (1998): Coarse-grain molecular dynamics and the atomic limit of finite elements. *Phys. Rev. B* 58: R5893-R5896.

Shen, S.; Atluri, S. N. (2004): Computational nano-mechanics and multiscale simulation. *CMC: Computers, Materials, & Continua* (in press)

Shenoy, V. B. (2003): Multiscale modeling strategies in materials science-the quasicontinuum method. *Bull. Mater. Sci*. 26(1): 53-62.

Srivastava, D.; Menon, M.; Cho, K. (2001): Computational nanotechnology with carbon nanotubes and fullerenes. *Computing in Science & Engineering* 3: 42-55.

Srivastava, D.; Atluri, S. N. (2002a): Computational Nanotechnology: A Current Perspective, *CMES: Computer Modeling in Engineering & Sciences* 3(5): 531-538

Srivastava, D.; Atluri, S. N. (2002b): Computational Nanotechnology, Special Issue, *CMES: Computer Modeling in Engineering & Sciences* 3(5).

Tadmor, E. B.; Oritz, M.; Phillips, R. (1996): Quasicontinuum analysis of defects in solids. *Philosophical Magazine* A 73: 1529-1563.

Tadmor, E. B.; Phillips, R.; Ortiz, M. (1996): Mixed atomistic and continuum models of deformation in solids. *Langmuir* 12(19): 4529-4534.

Tang, Z.; Shen, S.; Atluri, S. N. (2003): **Analysis of materials** with strain gradient effects: A Meshless local Petrov-Galerkin approach, with nodal displacements only. *CMES: Computer Modeling in Engineering & Sciences* 4(1): 177-196.

Tersoff, J. (1988): Empirical interatomic potential for carbon, with applications to amorphous carbon. *Phys. Rev. Lett*. 61(25): 2879-2882.

Tuckerman, M. E.; Berne, B. J.; Martyna, G. J. (1991): Molecular dynamics algorithm for multiple time scales: systems with long range forces. *J. Chem. Phys.* 94(10): 6811-6815.

Wagner, G. J.; Liu, W. K. (2003): Coupling of Atomistic and continuum simulations using a bridging scale decomposition. *J. Comput. Phys*. 190: 249-274.

Wendland, H. (1999): Meshless Galerkin method using radial basis functions. *Math. Comput*. 68: 1521-1531.

Zanzotto, G. (1996): The Cauchy-Born Hypothesis, nolinear elasticity and mechanical twinning in crystals. *Acta Cryst*. A52: 839-849.